Current Neuropharmacology, 2017, *15*, 1117-1135

RESEARCH ARTICLE

Chemoinformatics Profiling of the Chromone Nucleus as a MAO-B/A_{2A}AR Dual Binding Scaffold

Maykel Cruz-Monteagudo[a,b], Fernanda Borges[a,*], M. Natália D. S. Cordeiro[c], Aliuska Morales Helguera[d], Eduardo Tejera[b], Cesar Paz-y-Miño[b], Aminael Sánchez-Rodríguez[e], Yunier Perera-Sardiña[f] and Yunierkis Perez-Castillo[d,g,*]

[a]*CIQUP/Departamento de Química e Bioquímica, Faculdade de Ciências, Universidade do Porto, Porto 4169-007, Portugal;* [b]*Instituto de Investigaciones Biomédicas (IIB), Universidad de Las Américas, 170513 Quito, Ecuador;* [c]*REQUIMTE, Department of Chemistry and Biochemistry, Faculty of Sciences, University of Porto, 4169-007 Porto, Portugal;* [d]*Molecular Simulation and Drug Design Group, Centro de Bioactivos Químicos (CBQ), Universidad Central "Marta Abreu" de Las Villas, Santa Clara, 54830, Cuba;* [e]*Departamento de Ciencias Naturales, Universidad Técnica Particular de Loja, Calle París S/N, EC1101608 Loja, Ecuador;* [f]*Departamento de Ciencias Químicas, Facultad de Ciencias Exactas, Universidad Andres Bello, Santiago de Chile, Chile;* [g]*Sección Físico Química y Matemáticas, Departamento de Química, Universidad Técnica Particular de Loja, San Cayetano Alto S/N, EC1101608 Loja, Ecuador*

Abstract: ***Background*:** In the context of the current drug discovery efforts to find disease modifying therapies for Parkinson´s disease (PD) the current single target strategy has proved inefficient. Consequently, the search for multi-potent agents is attracting more and more attention due to the multiple pathogenetic factors implicated in PD. Multiple evidences points to the dual inhibition of the monoamine oxidase B (MAO-B), as well as adenosine A_{2A} receptor (A_{2A}AR) blockade, as a promising approach to prevent the neurodegeneration involved in PD. Currently, only two chemical scaffolds has been proposed as potential dual MAO-B inhibitors/A_{2A}AR antagonists (caffeine derivatives and benzothiazinones).

***Methods*:** In this study, we conduct a series of chemoinformatics analysis in order to evaluate and advance the potential of the chromone nucleus as a MAO-B/A_{2A}AR dual binding scaffold.

***Results*:** The information provided by SAR data mining analysis based on network similarity graphs and molecular docking studies support the suitability of the chromone nucleus as a potential MAO-B/A_{2A}AR dual binding scaffold. Additionally, a virtual screening tool based on a group fusion similarity search approach was developed for the prioritization of potential MAO-B/A_{2A}AR dual binder candidates. Among several data fusion schemes evaluated, the MEAN-SIM and MIN-RANK GFSS approaches demonstrated to be efficient virtual screening tools. Then, a combinatorial library potentially enriched with MAO-B/A_{2A}AR dual binding chromone derivatives was assembled and sorted by using the MIN-RANK and then the MEAN-SIM GFSS VS approaches.

***Conclusion*:** The information and tools provided in this work represent valuable decision making elements in the search of novel chromone derivatives with a favorable dual binding profile as MAO-B inhibitors and A_{2A}AR antagonists with the potential to act as a disease-modifying therapeutic for Parkinson´s disease.

ARTICLE HISTORY

Received: November 26, 2015
Revised: March 14, 2016
Accepted: November 03, 2016

DOI:
10.2174/1570159X15666170116145316

Keywords: A_{2A} adenosine receptor, chemoinformatics, chromones, dual-target binder, monoamine oxidase B, parkinson´s disease.

1. INTRODUCTION

Parkinson´s disease (PD) is the second most common age-related neurodegenerative disorder. The current yearly cost of healthcare for PD patients is estimated to exceed $ 5.6 billion just in the United States. With the increasing worldwide life expectancy, the prevalence of PD is projected to double by 2030 [1-3].

Currently, drugs based on dopamine replacement remain the main and most effective PD treatments [4]. However, their efficacy reduce as the disease progresses [5-7]. Ultimately, disease-modifying therapies addressing both the motor and non-motor symptoms of PD are needed.

*Address correspondence to these authors at the Departamento de Química. Universidad Técnica Particular de Loja. Loja. Ecuador;
E-mail: yperez@utpl.edu.ec and CIQUP/Departamento de Química e Bioquímica, Faculdade de Ciências, Universidade do Porto, Porto 4169-007, Portugal; Tel: (+351) 220402502; Fax: (+351) 220402659;
E-mail: fborges@fc.up.pt

Despite the increasing investment in biomedical research, the success rate of new drugs in clinical trials is falling, and PD is not the exception [8-12]. Academic and industry scientists acknowledge that the main efforts should be targeted to the drug discovery pipeline itself, particularly focusing on prioritizing and validating relevant targets and on evaluating candidate drugs [13]. So, novel drug targets are required to develop effective PD modifying treatments. On the other hand, since multiple genetic and environmental factors are involved in PD [14], the current single target strategy has proved ineffective. Thus, finding multi-potent agents is attracting more and more attention.

Inhibitors of the MAO-B enzyme are among the most common adjunctive drugs to the standard levodopa treatment of PD [15]. Oxidative deamination of many endogenous amines in the brain is catalyzed by MAO-B [16-18]. So, inhibition of this enzyme in the brain slows down the depletion of dopamine stores and elevates the levels of endogenously produced synaptic dopamine, as well as of dopamine derived from the exogenously administered levodopa [18, 19]. In addition, inhibitors of MAO may also exert a neuroprotective effect by decreasing the production of potentially hazardous catalytic by-products (including reactive oxygen species) of dopamine metabolism in the brain [20]. Considering that MAO-B activity in the human brain increases with age, it is evident the key role of MAO-B inhibition in PD [21-23].

In addition to MAO-B inhibitors, antagonists of the A_{2A} subtype of adenosine receptors (A_{2A}AR) are emerging as a new class of promising anti-parkinsonian agents [24-26]. Blockade of the A_{2A}AR in striatopallidal neurons potentiates dopamine 2 (D2) receptor mediated neurotransmission and therefore softens the effects of striatal dopamine depletion in PD [25, 27]. As a result, antagonism of the A_{2A}AR partially, but reliably, restores motor activity in animal models of PD [28]. Previous studies suggest that A_{2A}AR antagonism may also exert anti-parkinsonian effects which are independent from any D2 receptors mediated neurotransmission [29]. The antagonistic relationship between these receptors as a first point of departure and the distinctive distribution of A_{2A}AR in brain, constitute the basis for focusing on the A_{2A}AR antagonism as a disease modifying therapy for PD. These facts allow to assert that dual-target-directed drugs simultaneously inhibiting MAO-B and antagonizing A_{2A}AR, can have a significant value as disease-modifying agents in the management of PD.

The first success in the development of dual A_{2A}AR Antagonists/MAO-B Inhibitors as potential PD therapeutics came from studies on the MAO-B inhibition properties of a number of xanthinyl derived A_{2A}AR antagonists. These investigations were directed to test whether MAO-B inhibition contributed or not to the reported neuroprotective effect of A_{2A}AR antagonists [30, 31]. In addition to the evident structural relationship to adenosine, the natural endogenous ligand of ARs, several factors probably motivated the choice of caffeine as the scaffold for these studies. Previous reports of a reduced risk of developing PD associated to the consumption of caffeine can be identified as one of such motivating factors [32-34]. Also, recent reports of the neuroprotective effects in the 1-methyl-4-phenyl-1,2,3,6-tetrahydropyridine (MPTP) mouse model [35] of (E)-8-(3-chlorostyryl)caffeine (CSC) [36, 37], a selective A_{2A}AR antagonist, support the selection of caffeine.

The first attempt to depart from the caffeine scaffold was reported in [38] through a systematic modification of the caffeinyl core and substituents of the reference compound CSC. This research led to several 9-deazaxanthine derivatives exhibiting an excellent dual human A_{2A}AR antagonism/ MAO-B inhibition profile.

It was not until very recently that a real departure from the caffeine scaffold was successfully achieved by Müller and collaborators [39]. Based on a precedent study reporting the firsts non-caffeine-derived, non-adenine-related AR antagonists [40], Müller and colleagues evolved to the firsts potent, dual-target directed A_{2A}AR antagonists/MAO-B inhibitors with a non-caffeine scaffold. Actually, the best derivative obtained (the N-(4-oxo-4H-3,1-benzothiazin-2-yl)-4-phenylbutanamide) exhibited excellent A_{2A}AR antagonism/MAO-B inhibitory values below 50 nM, being selective too for the other subtypes of AR and monoamine oxidase A (MAO-A).

Although chromones are excellent MAO-B ligands, the A_{2A}AR antagonist capability of this chemical family is not so outstanding [41]. However, a potent A_{2A}AR antagonist with a chromone scaffold was recently discovered during a virtual screening (VS) study [42]. This recent finding suggests that the binding affinity of chromones for the A_{2A}AR can be modulated by placing proper structural modifications, while keeping the MAO-B inhibitory potency. In this study, we conduct a series of chemoinformatics analyses in order to evaluate and advance the potential of the chromone nucleus as a MAO-B/A_{2A}AR dual binding scaffold.

2. COMPUTATIONAL METHODS

2.1. SAR Data Mining based on Network-like Similarity Graphs

For the study of the main Structure-Activity Relationships (SAR) trends dominating the dual A_{2A}AR antagonists/ MAO-B inhibitors reported up to date we resort to SARANEA [43]. SARANEA is a freely available program implementing a graphical user interface to network similarity graphs (NSG) and NSG-based techniques for data mining.

2.1.1. SAR Data Collection

The SAR mapping based on NSG was applied to a subset of 63 compounds with reported values of half inhibitory concentration (IC_{50}) against the human MAO-B enzyme and of inhibition constant (K_i) of the human A_{2A}AR. This subset was compiled from [30, 38, 39] and it is provided as a SD file in the Supplementary Information. The file contains the respective molecular structures, MAO-B IC_{50} and A_{2A}AR K_i values in nanomolar units (nM), and the corresponding individual ($d_{MAO\text{-}B}$ and d_{A2aAR}) and overall (D_{Dual}) dual binding desirability values. The definitions of $d_{MAO\text{-}B}$, d_{A2aAR} and D_{Dual} are provided below.

2.1.2. Structure Codification

SARANEA uses as input customized molecular fingerprint representations. So, the freely available version of Molecular ACCess System (MACCS) structural keys [44]

implemented in the CDK software [45, 46] was used to represent the molecular structure of the 63 compounds analyzed.

2.1.3. Network-like Similarity Graphs

A dataset of chemical compounds can be represented through NSGs by showing all molecules and their similarity relationships. NSGs are graphs in which molecules are represented by nodes. Edges connecting individual nodes represent pair-wise similarity relationships. Only pairs of molecules exceeding a predefined threshold of similarity are connected by an edge. To visualize the distribution of potencies, nodes are coded by applying a continuous spectrum from green (lowest) to red (highest) potency. The compound discontinuity score codifies SAR characteristics of individual compounds and it is represented by node scaling representing the deviation in potency of a molecule from its structural neighbors. Large nodes reflect molecules inducing a high discontinuity and vice versa [47, 48]. Thus, it detects compounds introducing SAR discontinuity and activity cliffs. In NSGs, combinations of large green and red nodes linked by an edge are markers of activity cliffs that can be easily recognized. As previously mentioned, for this task we used SARANEA [43].

In SARANEA, a pair of connected compounds need to exceed a predefined Tanimoto coefficient (Tc) similarity threshold value. Here we applied a Tc similarity threshold of 0.65 to explore alternative routes to potent dual MAO-B/A_{2A}AR binders covering a broader range of structural scaffolds. SARANEA offers interactive access to the molecular representations through the nodes in the graph [43]. So, the SAR enclosed in the NSG can be easily explored with the aid of this feature.

SARANEA provides an additional set of functionalities to quantify compound-specific, local and global SAR features based on numerical functions. These functions codify pair-wise compound potency and similarity comparisons including the Cliff, and SAR (SARI) Indexes as well as the continuity and discontinuity scores [43, 49, 50]. These quantitative indexes can support the process of SAR mining. However, the calculation of this kind of functions includes standardization and normalization processes relying on a normalized set of molecules. So, we decided to prioritize those SARANEA features based on the graphic search of structure-similarity relationships.

The file supplied as input to SARANEA for the NSG analysis contains the list of the 63 compounds (48 caffeine derivatives and 15 benzothiazinones) including dual binding desirabilities and the corresponding molecular structures (see details in the next section). The binding affinities against the two targets of interest (MAO-B IC_{50} and A_{2A}AR K_i) were aggregated in a combined score by using a desirability function specifically adapted to represent the dual binding profile of the compounds under study.

2.1.4. Dual Binding Desirability

The desirability function was first proposed by Harrington [51] in 1965 as an approach for combining multiple responses in a single optimization equation. A desirability function maps the value of a property into a score ranging from zero to one which represents how desirable a case with this property value would be. Depending on the desired level for the target property, different desirability functions need to be applied. If a minimum value of the target property is desired, then a minimization desirability function is applied:

$$\boldsymbol{d_i} = \left[\frac{Y_i - U_i}{U_i - L_i}\right]^{s} \qquad \mathbf{0 < d_i < 1} \qquad \text{(eq. 1)}$$

If a maximum value of the target property is desired, then a maximization desirability function is applied:

$$\boldsymbol{d_i} = \left[\frac{Y_i - L_i}{L_i - U_i}\right]^{s} \qquad \mathbf{0 < d_i < 1} \qquad \text{(eq. 2)}$$

In equations 1 and 2, L and U are the minimum and maximum values of the property Y, respectively, while Y_i represents the value of the property for compound i. Moreover, the exponent s determines how significant is to hit the desired value (L or U).

If the property of a compound is beyond the ideal/unaccepted ranges, it will be scored with 1.0/0.0. Scores between 0 and 1 represent increasing desirability levels.

Once defined the desirability function for each property, the overall desirability D of candidate i can be estimated as the geometric mean of the individual desirability scores d as follows:

$$\boldsymbol{D_i} = \left(\prod_{i=1}^{n} \boldsymbol{d_i}\right)^{\frac{1}{n}} \qquad \mathbf{0 < D_i < 1} \qquad \text{(eq. 3)}$$

Thus, D provides the overall assessment of the desirability of the combined property levels. The range of D will fall in the interval [0, 1] and it will rise as the balance between the properties becomes more desirable, being 0 if at least one of the properties takes a value of $d = 0$.

Since a potent dual binding compound should exhibit low values of MAO-B IC_{50} and A_{2A}AR K_i, respectively, a minimization Derringer desirability function (equation 1) [52] was applied. This equation was specifically adapted for the visualization purposes of SARANEA. So, the minimum (desired) value L used for each property Y (MAO-B IC_{50} and A_{2A}AR K_i) corresponds to the value of MAO-B IC_{50}/A_{2A}AR K_i of the most potent MAO-B inhibitor/ A_{2A}AR antagonist (17.6 nM and 2.2 nM, respectively). The maximum value U of MAO-B IC_{50}/A_{2A}AR K_i was set to 100000 nM in both cases. The s parameter was adjusted for each property to render a corresponding d value = 0.5 for those compounds with MAO-B IC_{50}/A_{2A}AR K_i = 1000 nM (the threshold used for each target to consider a compound as a dual binder). This resulted in values of s of 70 and 69 for MAO-B IC_{50} and A_{2A}AR K_i respectively. In this way, only dual binding compounds will exhibit a d value for each target ($d_{MAO\text{-}B}$ and d_{A2aAR}, respectively) ≥ 0.5 and consequently, an overall *Dual Binding Desirability* (D_{Dual}) value ≥ 0.5.

The SARANEA input file is a zip folder containing a subfolder including the above mentioned information, and an additional subfolder including the files with the settings used for each applicable similarity threshold. Specifically, the D_{Dual} values corresponding to the 63 compounds analyzed

with the NSG approach were provided to SARANEA as [(1-D_{Dual})x1000] to fit the visualization requirements of the software. This zip file is provided as Supporting Information.

2.2. Molecular Docking

The SAR information extracted from the NSG-based SAR analysis of the benzothiazinones and caffeine derivatives reported in [30, 38, 39] guided the design of two chromone analogs. These analogs were based on the best dual MAO-B/A_{2A}AR benzothiazinone and caffeine derivative, respectively. The molecular structure of the chromone analogs and the corresponding dual MAO-B/A_{2A}AR benzothiazinone and caffeine derivatives are provided in Fig. (**1**).

A three dimensional conformer for each chromone analogue was generated using the ChemAxon's 3D coordinate/ conformer generation and analysis module (*Generate3D*) available in the MarvinSketch GUI. The geometry optimization performed by the *Generate3D* module is based on the Dreiding force-field [53] and started from a standardized 2D structure with explicit hydrogens, as described below in the *Data Curation and Standardization* section. Afterwards, charges were incorporated to each conformer by resorting to the ChemAxon's calculator (*cxcalc*) available also form the tools panel of the MarvinSketch GUI, considering the resonant structures and major microspecies at pH = 7.4.

The crystallographic structures of the A_{2A}AR in complex with the antagonist ZM241385 (PDB code 3PWH) and of the complex between MAO-B and a coumarin inhibitor (PDB code 2V61), were obtained from the Protein Data Bank (www.wwpdb.org). Receptor preparation was carried out with the UCSF Chimera software [54]. During receptor preparation all water molecules and ligands were removed and hydrogen atoms and charges were added. For both receptors the ligand binding pocket was defined as any residue lying at a distance below 5Å from the crystallographic ligand structure.

Molecular docking was performed with the DOCK v6.6 software [55] considering the ligand as flexible [56]. A maximum of 5000 conformations per ligand was explored allowing a maximum of two bumps between the receptor and the ligand. Bumps were defined as any pair of atoms closer than the 75% of the sum of their Van der Waals radii. The energy grid-based scoring function was chosen for the evaluation of poses quality. The top 20 lowest scored poses for each ligand were saved. To prevent redundancy on the predicted binding modes of each compound the resulting conformations were clustered using a threshold of 2 Å for the RMSD.

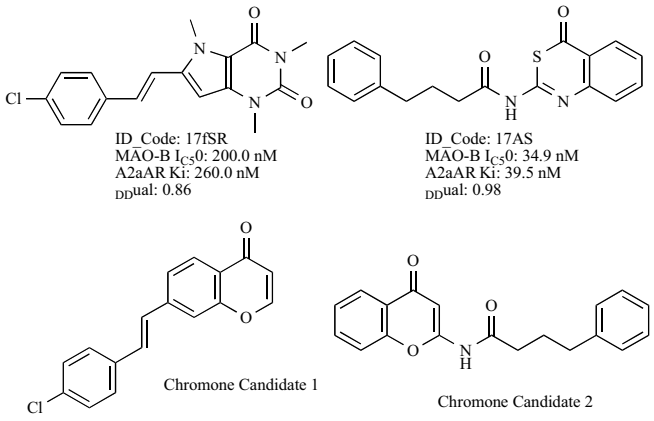

Fig. (1). Molecular structure of the chromone analogs used for molecular docking and the corresponding dual MAO-B/A_{2A}AR benzothiazinone and caffeine derivatives used as templates.

For interaction energies calculation, a grid was pre-computed for the receptor binding pocket region. The grid spacing was set to 0.3 Å and the attractive and repulsive Van der Waals coefficients were set to 6 and 12 respectively. Calculations were performed considering an all-atoms model. The obtained docking conformations were rescored using the GB/SA scoring function. This scoring function was selected because of its implicit solvent model and the fast calculation of the score for one ligand pose.

2.3. Group Fusion Similarity Search

2.3.1. Dual MAO-B/A2AAR Ligands and Decoys Data Collection

A set of sixteen dual MAO-B/A_{2A}AR ligands (caffeine derivatives and benzothiazinones) were compiled from [30, 38, 39]. Only compounds exhibiting values < 1000 nM of MAO-B IC_{50} and A_{2A}AR K_i were considered dual MAO-B/A_{2A}AR ligands. So, the remaining 48 caffeine derivatives and benzothiazinones were considered as dual MAO-B/A_{2A}AR decoys. An additional set of 32 chromones reporting human MAO-B IC_{50} and A_{2A}AR K_i values ≥ 1000 nM was compiled from [57-60] and used as dual MAO-B/A_{2A}AR decoys.

Additionally, dual MAO-B/A_{2A}AR decoys were extracted from individual MAO-B IC_{50} and A_{2A}AR K_i data, respectively. As dual MAO-B/A_{2A}AR decoys were considered only those compounds with MAO-B IC_{50} or A_{2A}AR K_i values ≥ 1000 nM. The human A_{2A}AR antagonists dataset was retrieved from the literature [57, 61-77]. It encompasses 327 compounds and contains nitrogen and oxygen heterocyles such as pyrazolo[3, 4-c]quinolines, 1,2,4-triazolo[4,3-a]quinoxalin-1-ones, pyrazolo-triazolo-pyrimidines, quinoxalines, mercaptopyrimidines, adenine derivatives, chromones and benzylketoindoles. The binding data was collected from different sources, but the protocols for competitive radioligand binding were similar. Only measurements using human A_{2A}AR subtype cloned in Chinese hamster ovary cells and [^{3}H]NECA as the radiolabeled ligand were considered. The spectrum of binding affinities (A_{2A}AR K_i values) ranged from 1.00 nM to >10000 nM. Only 191 compounds with A_{2A}AR K_i values ≥ 1000 nM were considered as dual MAO-B/A_{2A}AR decoys since their weak A_{2A}AR antagonist profile automatically exclude them as dual MAO-B/A_{2A}AR binders.

The human MAO-B inhibitor data was compiled from [58-60, 78-92]. It is composed by 474 compounds including different types of heterocycles such as chromones, coumarins, chalcones, 2-hydrazinylthiazoles, pyrazoles and homoisoflavonoids. All compounds were assayed for their inhibitory efficacy (IC_{50}) on the human MAO-B isoform following a single protocol, previously described in [93]. The spectrum

of *h*MAO-B inhibition ranged from 1.00 nM to > 100000 nM. Only 287 compounds with MAO-B IC_{50} values ≥ 1000 nM were considered as dual MAO-B/A_{2A}AR decoys since their weak MAO-B inhibitor profile automatically exclude them as dual MAO-B/A_{2A}AR binders.

Finally, a full set of 574 compounds comprising 16 dual MAO-B/A_{2A}AR ligands and 558 dual MAO-B/A_{2A}AR decoys was compiled. This dataset is provided as Supporting Information.

2.3.2. Data Curation and Standardization

The chemical structures of the 574 compounds collected from the literature were subject to standard curation procedures [94]. First, each SD file was generated using the JChem for Excel software [95]. The molecular structure representation was then standardized using ChemAxon´s Standardizer [96]. The parameters of the standardization process were set to obtain clean 2D molecular structures in SD format with benzenes in the aromatic form, explicit hydrogens, and a common representation (normalization) of specific chemotypes such as nitro or sulfoxide groups. The "*Find duplicate structures*" option of the EdiSDF program [97] included on the ISIDA project [98, 99] was used to detect and eliminate duplicate molecules.

2.3.3. Chemical Structure Codification and Chemical Similarity

The chemical structure of the 574 compounds was codified by the hashed chemical fingerprints (ChFP) implemented in the JChem for Excel program [95]. The chemical similarity relationships was established by using the Tanimoto coefficient as chemical similarity metric and ChFP as chemical reference space by resorting to the *JCDissimilarityCFTanimoto* function implemented in the JChem for Excel program [95].

2.3.4. Group Fusion Similarity Search

In the group fusion approach for similarity search (GFSS) [100], a user-defined set of structurally diverse reference structures (with the desired property/activity profile) is searched against a database using a common similarity measure. Here, the set of similarity values between each pair of reference and database compounds is combined into a new fused similarity score used to decreasingly rank the database. In this way, it is possible to "capture" the structural patterns determining the biological property under study.

In this work, the set of reference structures consists of five structurally diverse dual MAO-B/A_{2A}AR ligands. That is, among the sixteen dual MAO-B/A_{2A}AR ligands above described, the five compounds sharing the lowest structural similarity (using Tc based on ChFP) were selected. The molecular structure, identification code, MAO-B IC_{50} value, A_{2A}AR K_i value and dual binding desirability (D_{Dual}) value of each reference compound are depicted in Fig. (**2**).

The set of Tc similarity values between each reference dual MAO-B/A_{2A}AR ligand and each database compound is used to rank the compounds library (11 dual MAO-B/A_{2A}AR ligands and 558 dual MAO-B/A_{2A}AR decoys). Finally, several data fusion schemes are applied to obtain several fused similarity scores or fused ranks, which will be used as the definitive ranking criterion. The applied data fusion schemes were based on both, Tc similarity values and rank positions. Specifically, the maximum similarity (MAX-SIM), minimum similarity (MIN-SIM), mean similarity (MEAN-SIM), maximum rank (MAX-RANK), minimum rank (MIN-RANK) and mean rank (MEAN-RANK) data fusion schemes were applied [101].

2.3.5. Virtual Screening Performance

The primary goal in a virtual screening campaign is to select a subset from a large pool of candidates maximizing the number of known actives in this subset. Several enrichment metrics have been proposed to measure the enrichment ability of a VS tool. Here, we used some of the most extended metrics to evaluate the VS performance of the six different GFSS data fusion schemes and to select the best performing approach. These are: the area under the accumulative curve (*AUAC*), the area under the ROC curve (*ROC*), the enrichment factor (*EF*), the robust initial enhancement (*RIE*) and the Boltzmann-enhanced discrimination of ROC (*BEDROC*). See references [102, 103] for definition and interpretation details.

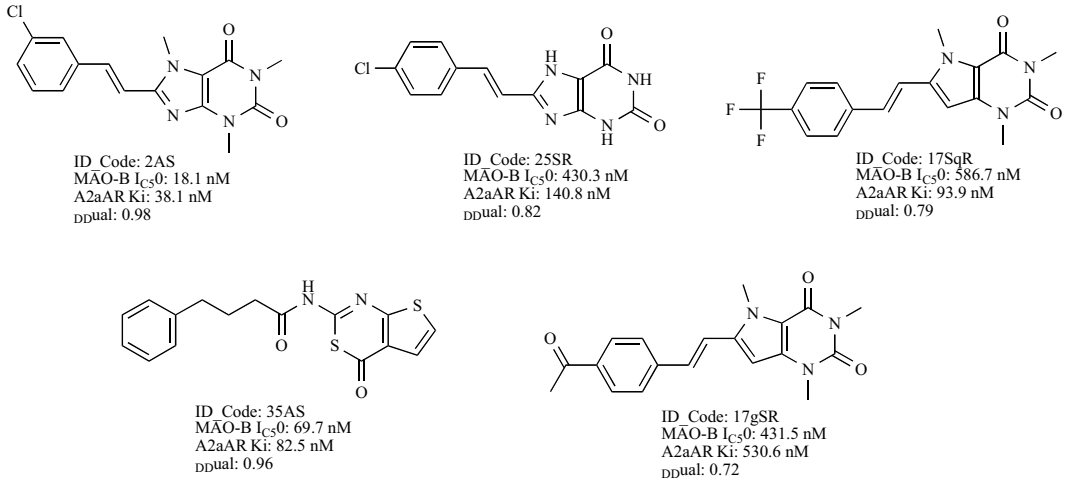

Fig. (2). Benzothiazinone and caffeine derivatives used as reference set for the GFSS virtual screening approach.

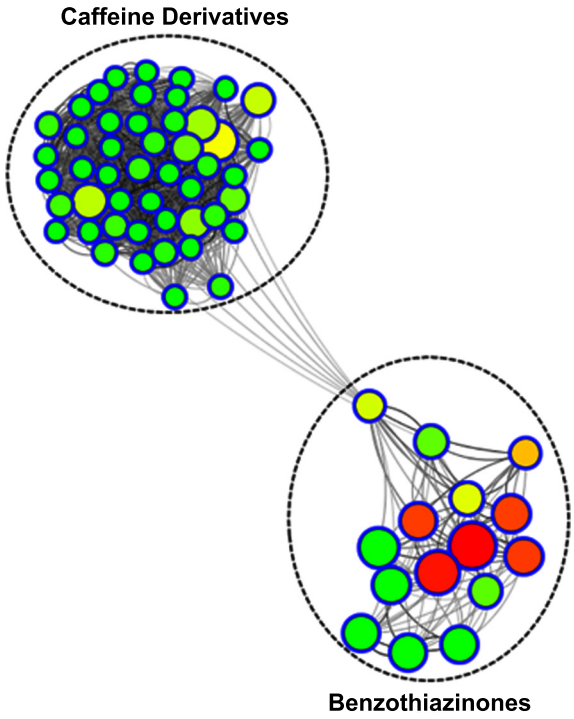

Fig. (3). NSG constructed with the software SARANEA for a join set of 48 caffeine derivatives and 15 benzothiazinones using a Tanimoto similarity threshold of 0.65. This NSG consists of two clusters encoding quite different local SARs. Nodes represent compounds connected by edges if they share a 2D similarity above a predefined threshold. The colour and size of a node reflect the dual binding desirability (D_{Dual}) value and contribution to the local SAR discontinuity of the corresponding compound, respectively.

3. RESULTS AND DISCUSSION

3.1. Network-like Similarity Graph Exploration of Current Dual MAO-B/A_{2A}AR Binders

The goal of the first analysis conducted was to visually detect highly discontinuous regions in the NSG encoding minimal structural changes that lead to significant variations in the dual binding profile, focusing on those containing activity cliffs. The compounds connected in this network share a structural similarity of 65% or higher. This network is characterized by the coexistence of regions with continuous and discontinuous SARs. Fig. **3** depicts the NSG obtained by applying as similarity threshold a Tc based on MACCS keys equals to 0.65. Regions of continuous SAR are characterized by clusters of small green nodes whereas discontinuous regions involve clusters composed of large green and red nodes. As deduced from Fig. **3**, this network contains similar subsets of molecules inducing SAR continuity and discontinuity, respectively. So, we can assert that at this similarity threshold, the molecules under study are characterized by a heterogeneous SAR. Similar and low continuity/discontinuity scores (0.264)/(0.140) determine a SARI index of 0.562, which supports the hypothesis of a heterogeneous relaxed SAR. This implies a SAR space moderately useful to extract relevant SAR information and to apply quantitative analyses based on chemical similarity.

As can be noted, the network obtained at this similarity threshold is a fully connected graph with two clusters clearly identified. A first cluster including 48 caffeine derivatives and a second one including 15 benzothiazinones. The cluster of caffeine derivatives is dominated by the presence of small green nodes among a few large yellow nodes. This is a clear indication of the contribution of this cluster to the continuity of the SAR of the human MAO-B/A_{2A}AR dual binding compounds under study. The presence of such a continuous SAR is a positive aspect for the application of similarity-based virtual screening methods to this family of compounds. However, these types of spaces are poor sources for extracting useful SAR information. So, from the visual inspection of the NSG, stringent criteria for dual binding are expected for caffeine derivatives.

A different space characterizes the bezothiazinones cluster, dominated by the presence of large green and red nodes. This clearly indicates that this cluster is the main contributor to the discontinuity of the global SAR. Contrary to the cluster of caffeine derivatives, this is a rich source to extract useful SAR information since any structural variation between two linked nodes leading to a significant alteration of the dual binding ability should come from a pair of compounds forming an activity cliff. Accordingly, such structural variations can be considered as relevant for establishing the SARs that characterize this chemical family. So, it is expected to find a wider structural variability contributing to the dual binding ability of benzothiazinones.

The previous analyses provide information on major SAR trends. Further analyses were applied by means of more advanced data structures implemented on SARANEA that mine the information contained in NSGs: SAR pathways and SAR trees.

3.1.1. NSG Based SAR Analysis of Caffeine Derivatives

To provide an overview of the SAR dominating the dual binding profile of caffeine derivatives, the pathways leading to or originating from a compound of interest can also be organized in a tree-like structure termed SAR tree [43, 104]. Therefore, to explore alternative routes to potent dual binding compounds (sequences of gradual structure modifications) covering a wide range of structural scaffolds, the cluster of caffeine derivatives was analyzed through the SAR tree utility.

To explore overall trends encoding different structural transitions from poor to potent dual binding caffeine derivatives, the respective SAR tree was constructed to originate from the caffeine derivative of highest dual binding ability. So, the obtained SAR tree is rooted at a yellow node representing the caffeine derivative of highest dual binding ability, and the leaves of the tree correspond to green nodes representing caffeine derivatives of low or null dual binding ability.

This SAR tree comprising the 48 caffeine derivatives analyzed (see Fig. **4**) provides a visual exploration of the overall pattern dominating the dual binding profile of caffeine derivatives. Here, it is possible to note that all the caffeine derivatives with at least a minimally acceptable dual binding profile (nodes **1**-**14** which exhibit a dual desirability value near to 0.5 or higher) share an 8-styryl moiety. Any

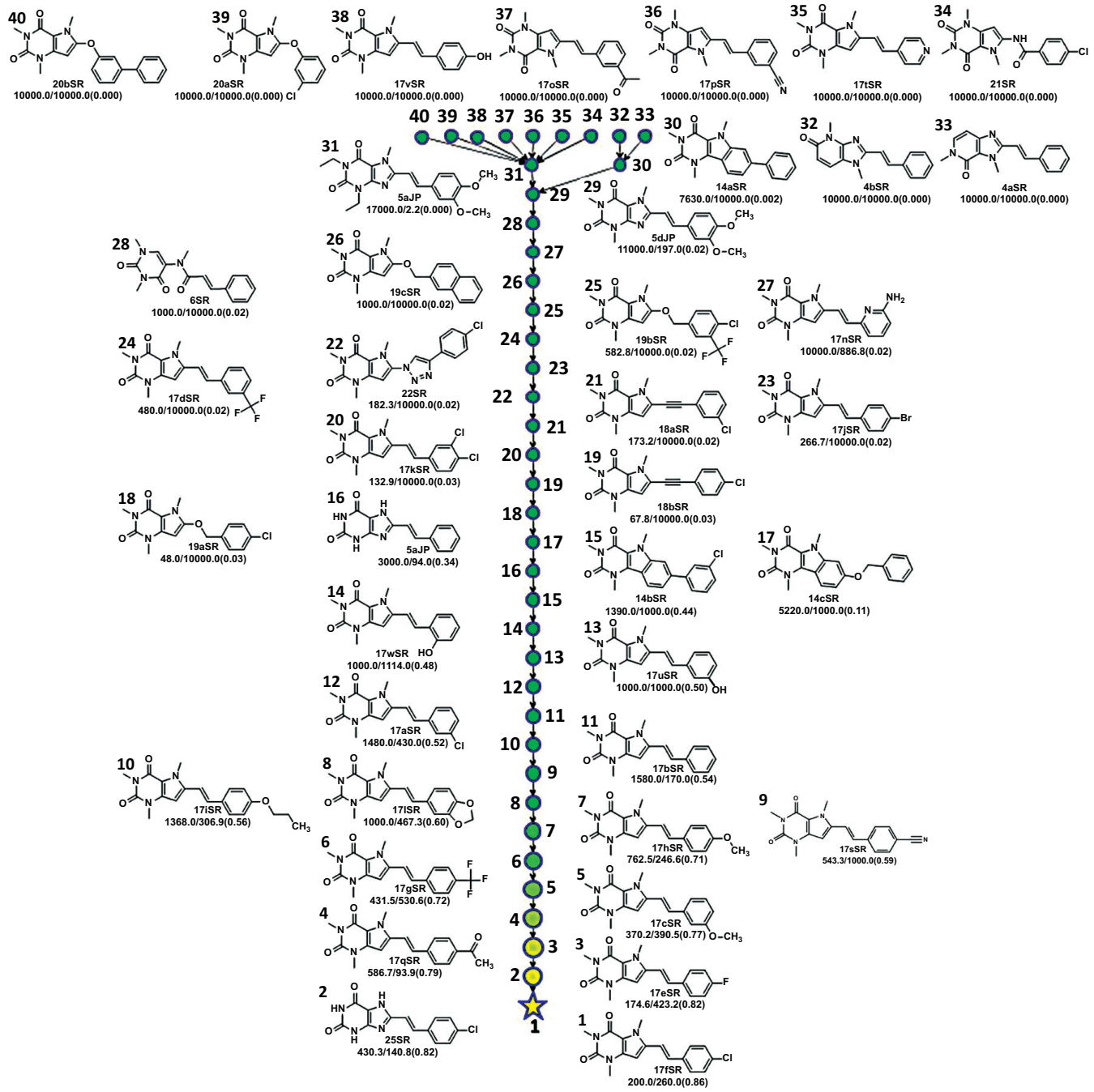

Fig. (4). SAR tree generated for cluster of 48 caffeine derivatives in the NSG obtained at a Tanimoto similarity threshold of 0.65. Green/yellow nodes represent compounds of low/high dual binding desirability. The molecular structures, MAO-B IC_{50}/A_{2A}AR K_i(D_{DUAL}) values of the caffeine derivatives represented by individual nodes in the SAR tree are shown.

spacer between the caffeine nucleus and the benzyl substituent different from ethenyl induces a significant loss of binding affinity over both or one of the targets. On the other hand, *para*-substitution of the styryl substituent with lipophilic, electron withdrawing groups, such as halogens or trifluoromethyl seems to induce a significant improvement of the binding affinity over both targets. A more detailed exploration of this pattern can be conducted by deriving SAR pathways focused on the SAR patterns of interest.

In Fig. (**5**) is provided a SAR pathway comprising representative caffeine derivatives in terms of spacer diversity. In this graph the molecular structure of the trimethyl-9-deazaxanthine derivatives containing the six main spacers (ethenyl, phenyl, methoxyl, ethynyl, triazolyl, formamidyl) linking a common *para*-chlorophenyl substituent are provided along their binding affinities to human MAO-B and A_{2A}AR. The D_{Dual} values are also provided in the scale bar. As can be noted, a deep loss on the dual binding ability is observed in

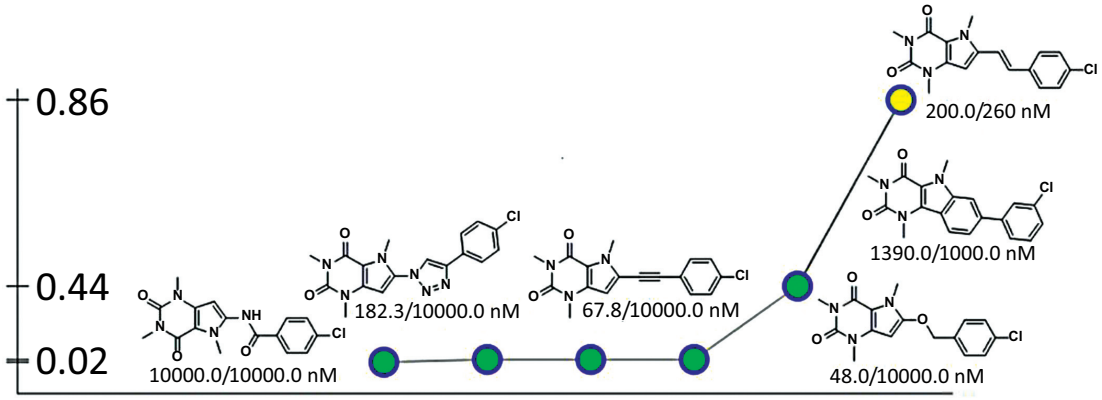

Fig. (5). SAR pathway comprising representative caffeine derivatives in terms of spacer diversity. Green/yellow nodes represent compounds of low/high dual binding desirability. Nodes are colour-coded and positioned in the graph according to the compound´s dual binding desirability (values provided in the scale bar). The molecular structures and the MAO-B $IC_{50}/A_{2A}AR$ K_i values of the caffeine derivatives represented by individual nodes in the SAR pathway are shown.

the caffeine derivatives with a spacer different of ethenyl. Although in most cases (derivatives with methoxyl, ethynyl, triazolyl spacers) potent MAO-B binders are obtained, a complete loss of $A_{2A}AR$ binding affinity is observed with any spacer different of ethenyl. So, the observed pattern indicates a critical role of ethenyl spacers in caffeine derivatives as dual MAO-B/$A_{2A}AR$ binders [38].

Once established the essential role of the ethynyl spacer, a SAR pathway analysis is conducted on the trimethyl-9-deazaxanthine derivatives with different substituents. First, by analyzing the dual binding profile (deduced from the respective D_{Dual} values) of nodes **1** to **6** in the SAR pathway graph (see Fig. **6**), it is possible to confirm the favorable effect of styryl substituents with lipophilic, electron withdrawing groups on the dual binding profile of caffeine derivatives as previously observed in the SAR tree analysis. Substituents such as chlorine, fluorine, acetyl and trifluoromethyl particularly improve the dual binding ability of 8-styryl-trimethyl-9-deazaxanthine derivatives when they are placed in *para* positions. The *meta*-substitution of the same groups induces a significant loss of the dual binding ability. The evolution of the dual binding profile of nodes **5** and **16** (D_{Dual} of node **5**/**16** = 0.72/0.02) as well as nodes **1** and **11** (D_{Dual} of node **1**/**11** = 0.86/0.52) are clear examples of the importance of the *para*-substitution for the dual binding ability of caffeine derivatives. On the other hand, the evolution of the dual binding profile of nodes **4**, **12**, and **13** evidences the detrimental effect of hydrophilic substituents.

3.1.2. NSG Based SAR Analysis of Benzothiazinones

An overview of the SAR dominating the dual binding profile of the 15 benzothiazinones under study can be accessed directly from the NSG. In Fig. **7** is provided a closer look at this cluster. Clusters of compounds that combine connected large red and green nodes can be regarded as activity cliff markers, which can be easily identified. So, this cluster was visually examined to identify the key SAR trends dominating this chemical family.

The most relevant activity cliff pair in this cluster (see Fig. **7**) is constituted by *N-(4-Oxo-4H-3,1-benzothiazin-2-*

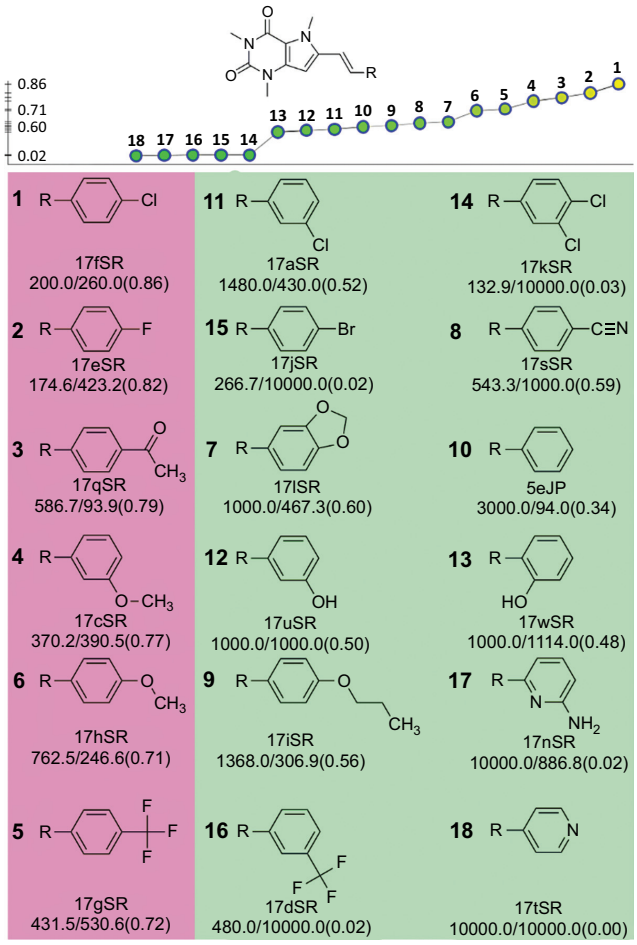

Fig. (6). SAR pathway comprising representative trimethyl-9-deazaxanthine derivatives with different substituents. Green/yellow nodes represent compounds of low/high dual binding desirability. Nodes are colour-coded and positioned in the graph according to the compound´s dual binding desirability (values provided in the scale bar). The molecular structures and the MAO-B $IC_{50}/A_{2A}AR$ $K_i(D_{DUAL})$ values of the caffeine derivatives represented by individual nodes in the SAR pathway are provided.

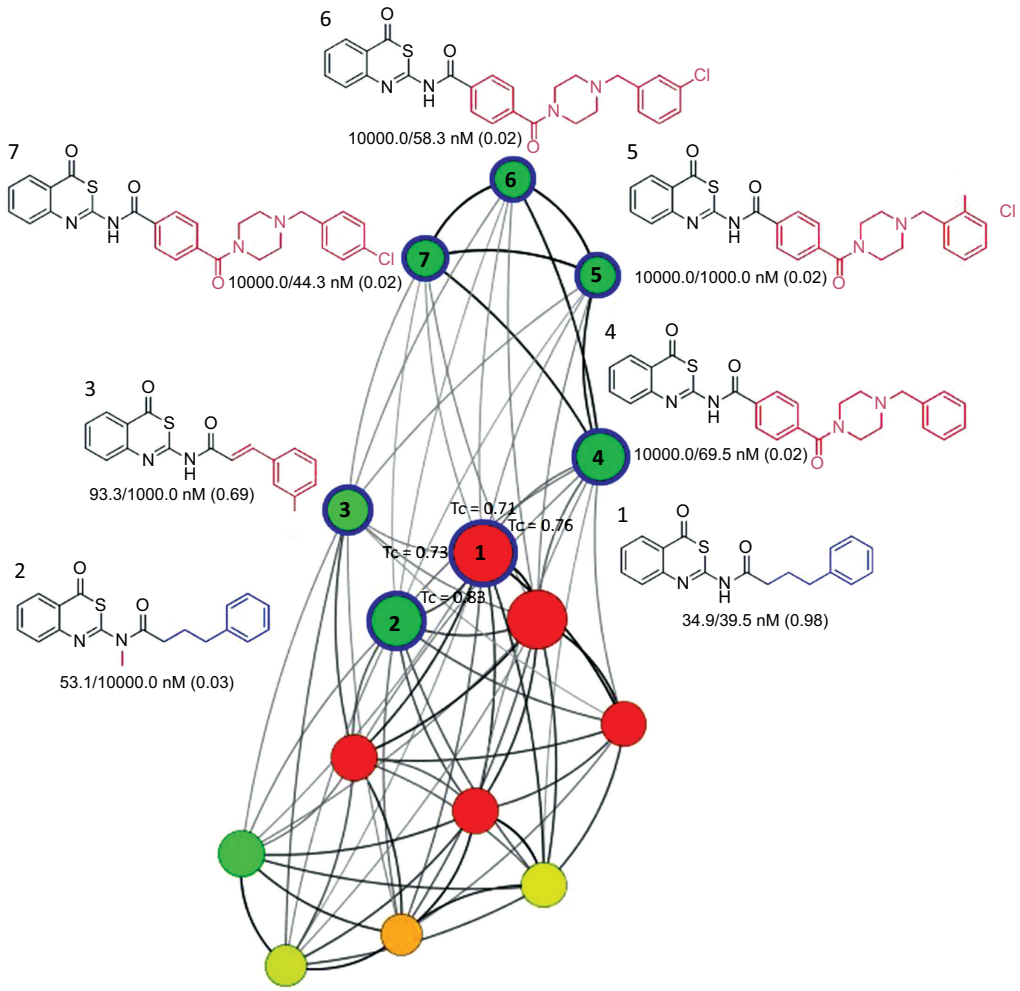

Fig. (7). Cluster of 15 benzothiazinones in the NSG constructed with the software SARANEA using a Tanimoto similarity threshold of 0.65. Nodes represent compounds connected by edges if they share a 2D similarity above a predefined threshold. The colour and size of a node reflect the dual binding desirability (D_{DUAL}) value and contribution to the local SAR discontinuity of the corresponding compound, respectively. The molecular structure of benzothiazinone analogs involved in activity cliffs are provided along their binding affinities on human MAO-B/A_{2A}AR. The DDual values are also provided (within parenthesis). Common/different molecular fragments are represented in black/blue or red.

yl)-4-phenylbutanamide, the most potent dual binding benzothiazinone and the N-methylated analogue *N-Methyl-N-(4-oxo-4H-3,1-benzothiazin-2-yl)-4-phenylbutanamide* (nodes **1** and **2**). The D_{Dual} value of **1** is 0.98 while the corresponding value of the N-methylated analogue **2** is significantly lower (0.03). This is reflected on a complete loss of A_{2A}AR affinity of the N-methylated analogue. On the other hand, the MAO-B affinity is conserved. This indicates that, although not critical for MAO-B binding, the amide proton may be necessary as hydrogen bond donor for A_{2A}AR binding [39], and consequently, essential for the dual binding ability.

Other trends are observed in this cluster of the NSG. From the activity cliff pair formed by nodes **1** and **3** it can be deduced that compounds with an unsaturated spacer and chloro substituents at the phenyl ring (node **3**) induce a significant loss of A_{2A}AR affinity (and consequently, a significantly lower dual binding ability) in comparison with unsubstituted analogs with saturated spacers (node **1**). On the other hand, the activity cliff pairs formed by nodes **4** to **7** with node **1** evidence that benzylpiperazine chloro-substituted or unsubstituted derivatives induce a significant loss of the dual binding ability due to a complete loss of MAO-B binding affinity.

The analysis of the SAR pathway corresponding to the benzothiazinone analogs aid to a deeper understanding of the general SAR trends observed in Fig. (**8**). In this figure the molecular structure of the benzothiazinone analogs are provided along with their binding affinities to human MAO-B/A_{2A}AR. The D_{Dual} values are also provided (within parenthesis) and represented in the scale bar.

Similarly high D_{Dual} values of compounds represented by nodes **1** (0.98) and **3** (0.93) suggest that the substitution of the benzothiazinone nucleus by a thiophenethiazinone nucleus does not affect the dual binding ability of unsubstituted analogs with saturated spacers. This observation supports the hypothesis that a certain degree of structural variability is allowed over the benzothiazinone nucleus without a significant loss of the dual binding ability.

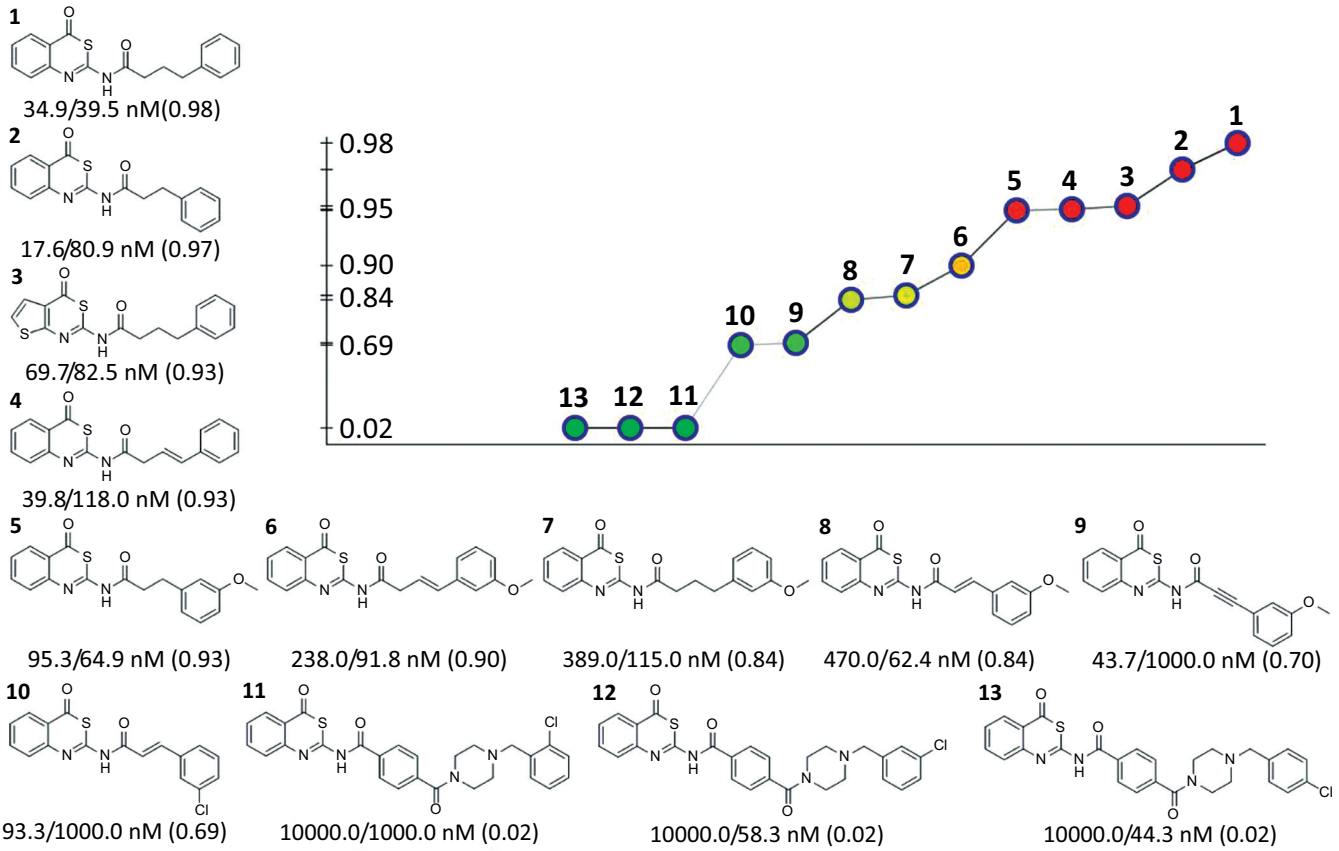

Fig. (8). SAR pathway comprising representative benzothiazinone analogs. Green/red nodes represent compounds of low/very high dual binding desirability. Nodes are colour-coded and positioned in the graph according to the compound´s dual binding desirability (values provided in the scale bar). The molecular structures and the MAO-B IC_{50}/$A_{2A}AR$ K_i(D_{DUAL}) values of the benzothiazinone analogs represented by individual nodes in the SAR pathway are provided.

The effect of the degree of unsaturation of the spacer can be deduced from the gradual deterioration of the dual binding ability form node **5** (ethyl spacer) to node **8** (ethenyl spacer) to node **9** (ethynyl spacer). This trend support the previous observation that benzothiazinone analogs with saturated spacers are well tolerated by both (MAO-B and $A_{2A}AR$) targets. The benzothiazinone analogs with better dual binding profiles are then characterized by short saturated spacers (ethyl or propyl) connected to unsubstituted or meta-methoxy substituted phenyl rings (nodes **1**, **2**, **3**, **5**, and **7** with D_{Dual} values higher than 0.84). In addition, these last phenyl substituents are also well tolerated when ethenyl spacers are used (nodes **4**, **6**, and **8**). Finally, chloro-phenyl substituents significantly reduce the $A_{2A}AR$ binding affinity and consequently affect the dual binding ability of benzothiazinone analogs (nodes **8** and **10**).

From the conducted SAR analysis of the two chemical families currently explored as MAO-B/$A_{2A}AR$ dual binders (benzothiazinones and caffeine derivatives), it is possible to infer that a limited number of chemical modifications are well tolerated by both targets. On the other hand, quite different substitutions patterns provided good binding affinities over both targets for each chemical family. Specifically, for the caffeine derivatives only an 8-styryl moiety (an ethenyl spacer between the caffeine nucleus and the phenyl ring) with a *para*-substitution of the styryl substituent with lipophilic, electron withdrawing groups, such as halogens or trifluoromethyl seems to induce a significant improvement of the binding affinity over both targets. On the other hand, for the benzothiazinones, more flexible spacers (propyl or ethyl) connecting an unsubstituted phenyl ring to a critical amide group at the C2 position of the benzothiazinone nucleus provided the best dual binding profile.

3.2. Molecular Modeling of the Chromone Nucleus as a Potential MAO-B/$A_{2A}AR$ Dual Binding Scaffold

Based on the SAR analyses provided above, we decided to evaluate the suitability of a chromone analogous to the best dual binding caffeine and benzothiazinone derivatives. For this, we resorted to the molecular docking of these two chromone derivatives candidates. As depicted in the *Molecular Docking* section both candidates were docked into the active site of each target (MAO-B and $A_{2A}AR$). The best pose obtained for each chromone candidate was compared with the respective co-crystalized ligand in order to access how much these candidates resemble the binding modes as well as critical interactions of known and potent ligands to the active site of their respective targets.

Fig. (**9**) shows the superposition, in stereo view, of the predicted binding mode of chromone candidates 1 and

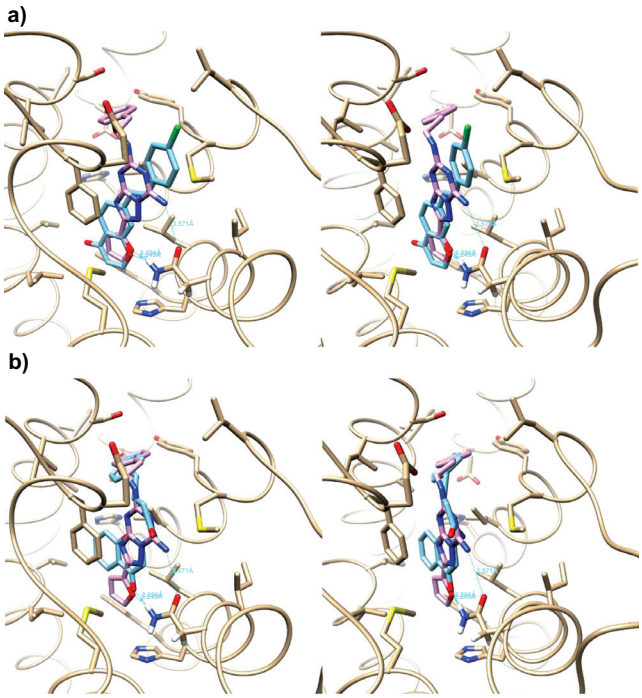

Fig. (9). Superposition, in stereo view, of the predicted binding mode of chromone candidates 1 (a) and 2 (b) to the A_{2A} adenosine receptor (PDB code 3PWH). The chromone candidates 1 and 2 are reported in cyan carbon sticks and the crystallographic ligand (ZM241385) is reported in magenta carbon sticks.

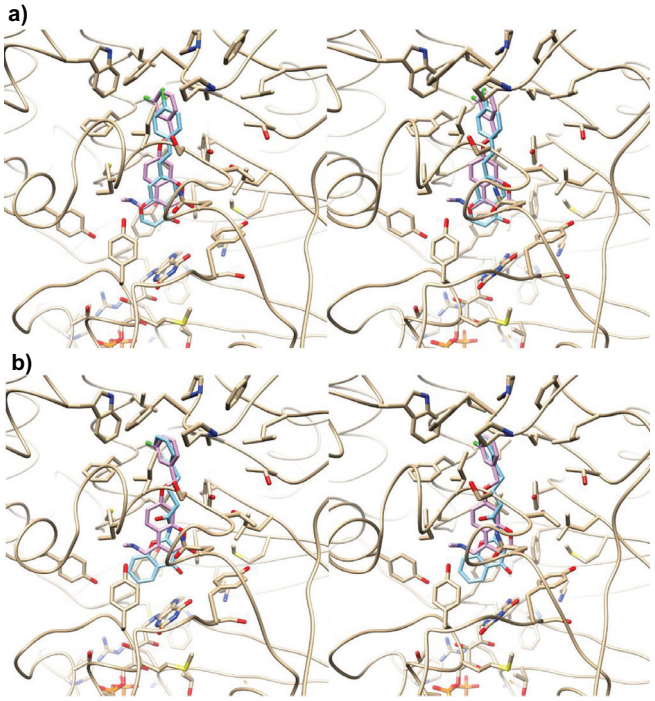

Fig. (10). Superposition, in stereo view, of the predicted binding mode of chromone candidates 1 (a) and 2 (b) to the MAO-B enzyme (PDB code 2V61). The chromone candidates 1 and 2 are reported in cyan carbon sticks and the crystallographic ligand (*7-(3-chlorobenzyloxy)-4-(methylamino)methyl-coumarin*) is reported in magenta carbon sticks.

2 to the A_{2A}AR, respectively. In both representations the crystallographic ligand was kept in order to compare its experimental binding mode with the predicted binding modes of both chromones. From this figure it can be seen that the binding mode of the both chromone analogs resemble that of the crystallographic ligand, occupying about the same region in the binding cavity as well as interacting with the same residues.

Two important interactions which are critical for the antagonist activity of ZM241385 [105] are conserved in both chromones. The first one is a hydrogen bond to ASN239 through the oxygen in position 1 of the chromone nucleus to the ASN amino group. The second important interaction is with TRP232 at the bottom of the binding tunnel which has been described as critical for other known $A2_AAR$ antagonists to achieve their activity. For the larger chromone candidate 2, it can be observed that in addition to keep the two mentioned critical interactions, the 4-phenylbutanamide moiety orients toward the same region as the analogous fragment of the crystallographic ligand.

On the other hand, it is well known that for MAO-B most interactions stabilizing the receptor-ligand complexes are Van der Waals and hydrophobic interactions. The predicted binding modes of the chromone candidates 1 and 2 to the MAO-B enzyme along with the crystallographic ligand (*7-(3-chlorobenzyloxy)-4-(methylamino)methyl-coumarin*) are provided in Fig. (**10**).

For this enzyme, the observed interactions correspond to what has been previously described for the binding of other bi-cyclic scaffolds to this target [41, 60, 106]. The chromone nucleus orientates facing the FAD co-factor and is stabilized in the binding tunnel by residues such as Gln206, Tyr398 and Tyr435 and by means of hydrophobic and van der Waals interactions, including π -π interactions with these tyrosine residues [92]. In both cases the substituent attached to the chromone scaffold orientates toward an upper hydrophobic sub-pocket which is exclusive of MAO-B and formed by Leu171, Ile199, Tyr326, Phe168, Ile316, Trp119, Pro102, and Pro104. According to previous studies [92], in addition to increasing the affinity of the ligand-receptor complexes, the interaction of the MAO-B inhibitors with residues in this sub-pocket is critical for the selectivity to this enzyme over MAO-A. The selective inhibition of the MAO-B enzyme exhibited by the compounds used as templates for the chromone analogs 1 and 2 (the caffeine derivative 17fSR and the benzothiazinone 17AS) supports this observation [38, 39].

The results provided by the conducted molecular docking analyses support the suitability of the chromone nucleus as a potential MAO-B/A_{2A}AR dual binding scaffold. So, these results grant a wider structural exploration focusing on this scaffold by assembling a combinatorial library enriched with potential dual binder chromones as well as the development of a VS tool for the prioritization of the most promising candidates.

3.3. Virtual Screening Tool for Dual MAO-B/A_{2A}AR Binders Based on a Group Fusion Similarity Search Approach

As previously described, six different fused scores coming from six data fusion schemes (MAX-SIM, MIN-SIM, MEAN-SIM, MAX-RANK, MIN-RANK and MEAN-RANK) were used as ranking criteria in order to find a convenient VS strategy for the automatic prioritization of dual MAO-B inhibitors/A_{2A}AR antagonists dispersed in a dataset of decoys. In doing so, we decided to simulate an experiment to assess the ability of the GFSS approach to retrieve just 11 dual MAO-B/A_{2A}AR ligands dispersed in 558 dual MAO-B/A_{2A}AR decoys collected from the literature.

This VS simulation set successfully fulfil the minimum requirements for a proper and unbiased estimation of the enrichment ability of a VS tool. First, it is composed by decoys which are in fact confirmed inactive compounds. On the other hand, the ratio of actives (dual ligands) R_a = 0.02 (52 decoys per ligand) of this dataset fulfil the minimum of 36 decoys proposed in [107].

Yet, we considered the relative error associated to the overall enrichment or early recognition metrics. In Table **1** are provided the relative errors associated to the enrichment metrics derived from this dataset as well as details on its size and composition. As can be noted from Table **1**, the relative error is not higher than 1% for most of the enrichment metrics, reaching a maximum of 7%. In fact, the enrichment metrics with associated relative errors around 3% are just those corresponding to the top 1% of the dataset, where the saturation effect becomes more critical. So, this data provides enough evidence to state that the effect of using this dataset does not significantly affects the inferences on the enrichment deduced from the enrichment metrics computed from it.

The first enrichment analysis based on the two metrics providing an overall picture of the VS performance (the *AUAC* and *ROC* metrics) of the six different variants of the GFSS approach suggests a promising performance of the GFSS approach, irrespective of the applied data fusion scheme. According to the values of these two metrics exhibited by the six data fusion schemes (see Table **2**), it is possible to infer that the similarity ranking provided by the GFSS approach is able to rank a dual MAO-B/A_{2A}AR ligand earlier than a dual MAO-B/A_{2A}AR decoy with a probability ranging between 0.73 (for the worst performing data fusion scheme) and 0.97 (for the best performing data fusion scheme). However, not every fusion scheme provided a favorable enrichment at the very early fractions of screened data. Only the MEAN-SIM and the MIN-RANK fusion schemes exhibited attractive *EF* values at this fraction. Both provided a top 1% fraction about 8 times more enriched with dual MAO-B/A_{2A}AR ligands than a random 1% fraction of the dataset. The rest of the schemes produced rankings not better than a random selection at this early fraction of screened data.

Table 1. Relative error associated to the enrichment metrics derived from the dataset used to estimate the enrichment performance of the GFSS approach.

Dataset Size and Composition			
N	*n*		R_a
558	11		0.0197
Relative Error (%) associated to Enrichment Metrics			
	EF	*RIE*	*BEDROC*
α = 160.9 (χ = 1%)	2.87	2.65	7.04
α = 32.2 (χ = 5%)	1.30	1.16	1.35
α = 16.1 (χ = 10%)	0.88	0.79	0.63
α = 8 (χ = 20%)	0.59	0.52	0.27
ROC	0.18		
AUAC	0.18		

At later fractions (top 5%, 10% and 20%) most of the fusion schemes exhibited favorable values of the *EF* metric, except for the MAX-SIM and MAX-RANK, which showed no enrichment at all. These results suggest an attractive overall (deduced from *ROC* and *AUAC*) and local (deduced from *EF*) enrichment ability of the GFSS approach. This is particularly true for the MEAN-SIM and the MIN-RANK fusion schemes. This assertion can be confirmed by visually inspecting the ROC curves of the six data fusion schemes employed under the GFSS approach, which are provided in Fig. **11**. From Fig. **11**, specifically from the zoom made to the top 5% fraction, it is possible to note that it is in this fraction where the enrichment ability of the two best performing fusion schemes (MEAN-SIM and the MIN-RANK) focusses. In general, as expected from previous studies on the VS performance of different data fusion schemes [101], the MIN-RANK fusion exhibited the best VS performance. However, contrary to these studies, the MAX-SIM exhibited a rather poor VS performance.

Nevertheless, classic enrichment metrics, such as *ROC*, *AUAC* and *EF*, cannot distinguish between a VS approach that ranks half of the actives at the top of the ordered list and the second half at the bottom from a VS protocol that ranks all actives at the top of the list. This feature is known as "early recognition" ability and is the most significant property of a VS approach. Therefore, the analysis of metrics such as *BEDROC* and *RIE* are crucial to efficiently estimate this critical feature on a VS protocol, particularly when very large datasets are intended to be screened.

The analysis of *RIE* at the respective top 1%, 5%, 10% and 20% fractions allows to deduce that the early recognition ability of all the data fusion schemes follows a behavior similar to that observed for the *EF* metric. The MEAN-SIM and the MIN-RANK fusion schemes stand up among the rest of the schemes as those with best early recognition ability. Although the MIN-RANK schemes looks like the most promising one, the early recognition ability of the MEAN-SIM scheme at very early fractions (top 1%) suggests a better performance of this one for the VS of large chemical libraries. On the contrary, the significantly better early recognition ability of the MIN-RANK scheme makes it

Table 2. Virtual screening performance metrics of the six different data fusion variants of the GFSS approach.[a]

	MIN-SIM	MAX-SIM	MEAN-SIM
Classic Enrichment Metrics			
AUAC	0.9497(±0.0017)	0.7254(±0.0013)	0.8768(±0.0016)
ROC	0.9585(±0.0017)	0.7298(±0.0013)	0.8842(±0.0016)
$EF_{1\%}$	0.0000(±0.0000)	0.0000(±0.0000)	**8.6212(±0.2471)**
$EF_{5\%}$	8.9185(±0.1159)	0.0000(±0.0000)	6.4659(±0.0841)
$EF_{10\%}$	**9.9825(±0.0884)**	0.0000(±0.0000)	3.4485(±0.0305)
$EF_{20\%}$	**4.9912(±0.0294)**	0.9075(±0.0054)	3.8475(±0.0227)
Early Recognition Metrics			
$RIE_{1\%}$	4.4877(±0.1191)	0.0000(±0.0000)	**11.6503(±0.3108)**
$RIE_{5\%}$	8.9998(±0.1045)	0.0420(±0.0005)	7.0358(±0.0817)
$RIE_{10\%}$	7.8825(±0.0625)	0.3884(±0.0031)	5.1171(±0.0406)
$RIE_{20\%}$	5.4987(±0.0285)	1.0757(±0.0056)	3.7904(±0.0196)
$BEDROC_{1\%}$	0.0908(±0.0064)	0.0000(±0.0000)	**0.2357(±0.0166)**
$BEDROC_{5\%}$	0.3755(±0.0051)	0.0018(±0.0000)	0.2935(±0.0040)
$BEDROC_{10\%}$	0.5697(±0.0036)	0.0281(±0.0002)	0.3699(±0.0023)
$BEDROC_{20\%}$	0.7415(±0.0020)	0.1447(±0.0004)	0.5110(±0.0014)
	MIN-RANK	**MAX-RANK**	**MEAN-RANK**
Classic Enrichment Metrics			
AUAC	**0.9649(±0.0018)**	0.7373(±0.0014)	0.7603(±0.0014)
ROC	**0.9740(±0.0018)**	0.7420(±0.0013)	0.7655(±0.0014)
$EF_{1\%}$	**8.6212(±0.2471)**	0.0000(±0.0000)	0.0000(±0.0000)
$EF_{5\%}$	**14.2696(±0.1855)**	0.0000(±0.0000)	7.1348(±0.0927)
$EF_{10\%}$	**9.9825(±0.0884)**	0.0000(±0.0000)	3.6300(±0.0322)
$EF_{20\%}$	**4.9912(±0.0294)**	0.9075(±0.0054)	1.8150(±0.0107)
Early Recognition Metrics			
$RIE_{1\%}$	7.3543(±0.1952)	0.0000(±0.0000)	0.4407(±0.0117)
$RIE_{5\%}$	**12.2781(±0.1425)**	0.0185(±0.0002)	3.7784(±0.0439)
$RIE_{10\%}$	**9.6143(±0.0763)**	0.3116(±0.0025)	3.3290(±0.0264)
$RIE_{20\%}$	**6.1392(±0.0318)**	1.0574(±0.0055)	2.5035(±0.0130)
$BEDROC_{1\%}$	0.1488(±0.0105)	0.0000(±0.0000)	0.0089(±0.0006)
$BEDROC_{5\%}$	**0.5122(±0.0069)**	0.0008(±0.0000)	0.1576(±0.0021)
$BEDROC_{10\%}$	**0.6949(±0.0044)**	0.0225(±0.0001)	0.2406(±0.0015)
$BEDROC_{20\%}$	**0.8279(±0.0022)**	0.1423(±0.0004)	0.3374(±0.0009)

[a]: The relative error associated to each enrichment metric is reported. *AUAC*: area under the accumulation curve; *ROC*: area under the ROC curve; $EF_{1\%/5\%/10\%/20\%}$: enrichment factor at top 1%/5%/10%/20% fraction, respectively; $RIE_{1\%/5\%/10\%/20\%}$: robust initial enhancement at top 1%/5%/10%/20% fraction, respectively; $BEDROC_{1\%/5\%/10\%/20\%}$: Boltzmann-enhanced discrimination of ROC at top 1%/5%/10%/20% fraction, respectively.

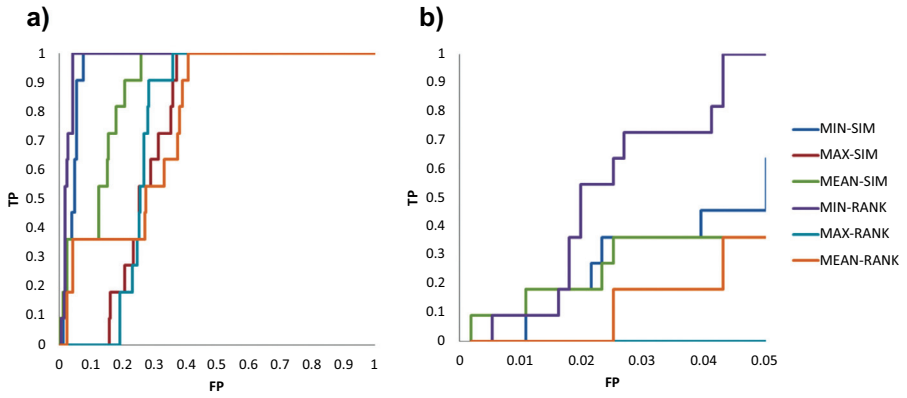

Fig. (11). ROC curves obtained from the application of the six different data fusion variants of the GFSS approach to the virtual screening of a subset of 11 dual MAO-B/A_{2A}AR ligands from 563 decoys (a). A zoom at the top 5% fraction is also provided (b). Here TP and FP accounts for the true positive ratio and false positive ratio, respectively.

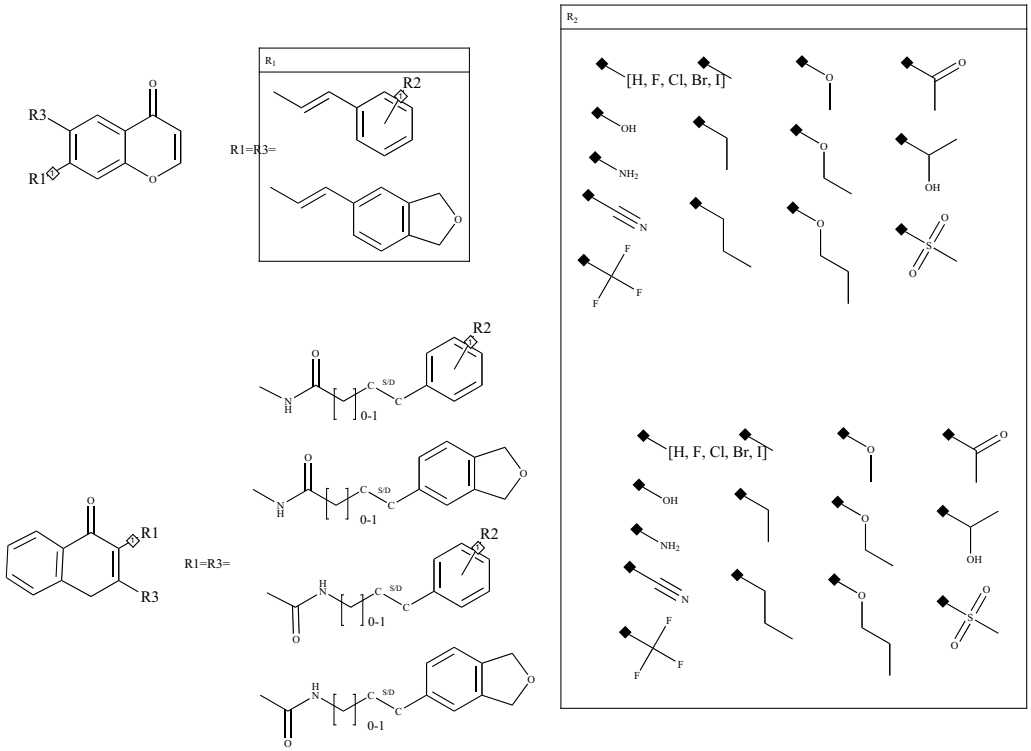

Fig. (12). Scheme applied to assemble the focused combinatorial library.

better suited for the VS of smaller chemical libraries where larger fractions (top 5% - 20%) can be assayed.

This behavior is also observed when considering *BEDROC*. The probabilistic interpretation of *BEDROC* allows to confirm that the capacity of the MEAN-SIM scheme (BEDROC = 0.24) to rank most of the dual MAO-B/A_{2A}AR ligands at the beginning of the filtered fraction is steadily superior to the MIN-RANK scheme (BEDROC =0.15). In other words, the MEAN-SIM scheme almost doubles the early recognition ability of the MIN-RANK scheme in the top 1% fraction of screened data (see Table **2**). However, the higher values of the *BEDROC* metric exhibited by the MIN-RANK scheme at later filtered fractions (top 5% - 20%) clearly points to this fusion scheme as the best candidate in comparison to the MEAN-SIM scheme.

Summarizing, we can conclude that MEAN-SIM and MIN-RANK GFSS schemes are valid options as VS tools. Thus, for the screening of moderately large libraries (hundreds or even thousands) were a top fraction between 5% and 20% of the compounds is intended to be experimentally evaluated, the MIN-RANK GFSS scheme should lead to the identification of a significant number of dual MAO-B/A_{2A}AR ligands. Instead, if only the top 1% of a considerably larger virtual library (thousands or millions) must be considered, the MIN-RANK GFSS approach is expected to render an attractive enrichment performance.

Even so, the combined use of both approaches should also render a positive enrichment performance in a wider range of VS scenarios.

3.4. Focused Combinatorial Library Potentially Enriched with Dual Binding Chromones

Finally, the SAR and molecular modeling analyses provided the information required to obtain a combinatorial library potentially enriched with MAO-B/A_{2A}AR dual binding chromone derivatives. At the same time, the proposed GFSS VS approach can be used to efficiently prioritize the chromone derivatives with the most promising dual binding profile.

Although both types of nucleuses have proved to be effective for MAO-B/A_{2A}AR dual binding, the NSG-based analyses conducted on these two chemical families suggest quite different substitution patterns favoring the dual binding ability. So, in order to assemble our combinatorial library, different substitution patterns should be applied to the chromone nucleus, depending on the SAR dominating each chemical family. The *Markush Enumeration* function available in the MarvinSketch GUI was employed to assemble a focused combinatorial library according to the scheme illustrated in Fig. (**12**). The final outcome is a focused combinatorial library of 956 chromone derivatives structurally enriched with substitutions patterns providing a potentially favorable dual binding profile. These substitutions were deduced from the NSG analyses previously detailed. Substituents other than only those resulting in a favorable dual binding profile were also considered in order to explore a wider structural space.

The combinatorial library of chromone derivatives sorted by using the proposed MIN-RANK and then the MEAN-SIM GFSS VS approaches is provided as a supplementary material. This combinatorial library represents a practical decision making tool in the search for novel chromone derivatives with a favorable dual binding profile as MAO-B inhibitors and A_{2A}AR antagonists.

CONCLUSION

Several chemoinformatics analyses were conducted in this work in order to profile the potential of the chromone nucleus as a dual MAO-B/A_{2A}AR scaffold. From the NSG-based SAR analysis conducted on the two chemical families currently explored as MAO-B/A_{2A}AR dual binders (benzothiazinones and caffeine derivatives), it was possible to infer that a limited number of chemical modifications are well tolerated by both targets. On the other hand, quite different substitutions patterns provided good binding affinities over both targets for each chemical family. Specifically, for the caffeine derivatives only an 8-styryl moiety (an ethenyl spacer between the caffeine nucleus and the phenyl ring) with a *para*-substitution of the styryl substituent with lipophilic, electron withdrawing groups, such as halogens or trifluoromethyl seems to induce a significant improvement of the binding affinity over both targets. On the other hand, for the benzothiazinones, more flexible spacers (propyl or ethyl) connecting an unsubstituted phenyl ring to a critical amide group at the C2 position of the benzothiazinone nucleus provided the best dual binding profile.

Based on the results of the SAR analyses, we tested the suitability of a chromone analogue of the best dual binding caffeine derivative and benzothiazinone, respectively. For this we resorted to the molecular docking of these two chromone derivatives candidates. Both chromone analogs were docked into the active site of each target (MAO-B and A_{2A}AR) and the best pose obtained was compared with the respective co-crystalized ligand. The results provided by this molecular docking analyses showed that the best pose obtained for each chromone analogue resembles the binding mode as well as reproduces critical interactions of known and potent ligands to the active site of the respective target. These results support the suitability of the chromone nucleus as a potential MAO-B/A_{2A}AR dual binding scaffold.

Additionally, a virtual screening tool based on a group fusion similarity search approach was developed for the prioritization of potential MAO-B/A_{2A}AR dual binder candidates. Among the six different data fusion schemes evaluated, the MEAN-SIM and MIN-RANK GFSS approaches demonstrated to be perfectly valid options as VS tools. Then, a combinatorial library potentially enriched with MAO-B/A_{2A}AR dual binding chromone derivatives was assembled and sorted by using the MIN-RANK and then the MEAN-SIM GFSS VS approaches.

Finally, the compendium of SAR data, molecular modeling analysis, virtual screening tools and the combinatorial library provided in this work represents valuable decision making elements to aid medicinal chemists in the search of novel chromone derivatives with a favorable dual binding profile as MAO-B inhibitors and A_{2A}AR antagonists, with the potential to act as a disease-modifying therapeutic for Parkinson´s disease.

ETHICS APPROVAL AND CONSENT TO PARTICIPATE

Not applicable.

HUMAN AND ANIMAL RIGHTS

No Animals/Humans were used for studies that are base of this research.

CONSENT FOR PUBLICATION

Not applicable.

CONFLICT OF INTEREST

The authors declare no conflict of interest, financial or otherwise.

ACKNOWLEDGEMENTS

MC-M acknowledges the postdoctoral grant [SFRH/BPD/90673/2012] financed by the FCT – Fundação para a Ciência e a Tecnologia, Portugal, co-financed by the European Social Fund. YP-S thanks Universidad Andres Bello for funding this work through PhD in Molecular Physical Chemistry.

SUPPLEMENTARY MATERIAL

Supplementary material is available on the publisher's web site along with the published article.

REFERENCES

[1] Olanow, C.W.; Stern, M.B.; Sethi, K. The scientific and clinical basis for the treatment of Parkinson disease (2009). *Neurology,* **2009**, *72*(21)(Suppl. 4), S1-S136. [http://dx.doi.org/10.1212/WNL.0b013e3181a1d44c] [PMID: 19470958]

[2] de Lau, L.M.; Giesbergen, P.C.; de Rijk, M.C.; Hofman, A.; Koudstaal, P.J.; Breteler, M.M. Incidence of parkinsonism and Parkinson disease in a general population: the Rotterdam Study. *Neurology,* **2004**, *63*(7), 1240-1244. [http://dx.doi.org/10.1212/01.WNL.0000140706.52798.BE] [PMID: 15477545]

[3] Dorsey, E.R.; Constantinescu, R.; Thompson, J.P.; Biglan, K.M.; Holloway, R.G.; Kieburtz, K.; Marshall, F.J.; Ravina, B.M.; Schifitto, G.; Siderowf, A.; Tanner, C.M. Projected number of people with Parkinson disease in the most populous nations, 2005 through 2030. *Neurology,* **2007**, *68*(5), 384-386. [http://dx.doi.org/10.1212/01.wnl.0000247740.47667.03] [PMID: 17082464]

[4] Cotzias, G.C.; Van Woert, M.H.; Schiffer, L.M. Aromatic amino acids and modification of parkinsonism. *N. Engl. J. Med.,* **1967**, *276*(7), 374-379. [http://dx.doi.org/10.1056/NEJM196702162760703] [PMID: 5334614]

[5] Braak, H.; Del Tredici, K.; Rüb, U.; de Vos, R.A.; Jansen Steur, E.N.; Braak, E. Staging of brain pathology related to sporadic Parkinson's disease. *Neurobiol. Aging,* **2003**, *24*(2), 197-211. [http://dx.doi.org/10.1016/S0197-4580(02)00065-9] [PMID: 12498954]

[6] Zarow, C.; Lyness, S.A.; Mortimer, J.A.; Chui, H.C. Neuronal loss is greater in the locus coeruleus than nucleus basalis and substantia nigra in Alzheimer and Parkinson diseases. *Arch. Neurol.,* **2003**, *60*(3), 337-341. [http://dx.doi.org/10.1001/archneur.60.3.337] [PMID: 12633144]

[7] Hawkes, C.H.; Del Tredici, K.; Braak, H. A timeline for Parkinson's disease. *Parkinsonism Relat. Disord.,* **2010**, *16*(2), 79-84. [http://dx.doi.org/10.1016/j.parkreldis.2009.08.007] [PMID: 19846332]

[8] Morgan, S.; Grootendorst, P.; Lexchin, J.; Cunningham, C.; Greyson, D. The cost of drug development: a systematic review. *Health Policy,* **2011**, *100*(1), 4-17. [http://dx.doi.org/10.1016/j.healthpol.2010.12.002] [PMID: 21256615]

[9] Paul, S.M.; Mytelka, D.S.; Dunwiddie, C.T.; Persinger, C.C.; Munos, B.H.; Lindborg, S.R.; Schacht, A.L. How to improve R&D productivity: the pharmaceutical industry's grand challenge. *Nat. Rev. Drug Discov.,* **2010**, *9*(3), 203-214. [PMID: 20168317]

[10] Lou, K.; de Rond, M. The 'not invented here' myth. *Nat. Rev. Drug Discov.,* **2006**, *5*(6), 451-452. [http://dx.doi.org/10.1038/nrd2063] [PMID: 16821286]

[11] Müller, T. New small molecules for the treatment of Parkinson's disease. *Expert Opin. Investig. Drugs,* **2010**, *19*(9), 1077-1086. [http://dx.doi.org/10.1517/13543784.2010.504711] [PMID: 20645881]

[12] Goetz, C.G.; Damier, P.; Hicking, C.; Laska, E.; Müller, T.; Olanow, C.W.; Rascol, O.; Russ, H. Sarizotan as a treatment for dyskinesias in Parkinson's disease: a double-blind placebo-controlled trial. *Mov. Disord.,* **2007**, *22*(2), 179-186. [http://dx.doi.org/10.1002/mds.21226] [PMID: 17094088]

[13] Nolan, G.P. What's wrong with drug screening today. *Nat. Chem. Biol.,* **2007**, *3*(4), 187-191. [http://dx.doi.org/10.1038/nchembio0407-187] [PMID: 17372598]

[14] Lee, F.J.; Liu, F. Genetic factors involved in the pathogenesis of Parkinson's disease. *Brain Res. Brain Res. Rev.,* **2008**, *58*(2), 354-364. [http://dx.doi.org/10.1016/j.brainresrev.2008.02.001] [PMID: 18313759]

[15] Fernandez, H.H.; Chen, J.J. Monoamine oxidase-B inhibition in the treatment of Parkinson's disease. *Pharmacotherapy,* **2007**, *27*(12 Pt 2), 174S-185S. [http://dx.doi.org/10.1592/phco.27.12part2.174S] [PMID: 18041937]

[16] Youdim, M.B.; Collins, G.G.; Sandler, M.; Bevan Jones, A.B.; Pare, C.M.; Nicholson, W.J. Human brain monoamine oxidase: multiple forms and selective inhibitors. *Nature,* **1972**, *236*(5344), 225-228. [http://dx.doi.org/10.1038/236225b0] [PMID: 4553640]

[17] Collins, G.G.; Sandler, M.; Williams, E.D.; Youdim, M.B. Multiple forms of human brain mitochondrial monoamine oxidase. *Nature,* **1970**, *225*(5235), 817-820. [http://dx.doi.org/10.1038/225817a0] [PMID: 5415111]

[18] Di Monte, D.A.; DeLanney, L.E.; Irwin, I.; Royland, J.E.; Chan, P.; Jakowec, M.W.; Langston, J.W. Monoamine oxidase-dependent metabolism of dopamine in the striatum and substantia nigra of L-DOPA-treated monkeys. *Brain Res.,* **1996**, *738*(1), 53-59. [http://dx.doi.org/10.1016/0006-8993(96)00761-5] [PMID: 8949927]

[19] Finberg, J.P.; Wang, J.; Bankiewicz, K.; Harvey-White, J.; Kopin, I.J.; Goldstein, D.S. Increased striatal dopamine production from L-DOPA following selective inhibition of monoamine oxidase B by R(+)-N-propargyl-1-aminoindan (rasagiline) in the monkey. *J. Neural Transm. Suppl.,* **1998**, *52*, 279-285. [http://dx.doi.org/10.1007/978-3-7091-6499-0_28] [PMID: 9564628]

[20] Youdim, M.B.; Bakhle, Y.S. Monoamine oxidase: isoforms and inhibitors in Parkinson's disease and depressive illness. *Br. J. Pharmacol.,* **2006**, *147*(Suppl. 1), S287-S296. [http://dx.doi.org/10.1038/sj.bjp.0706464] [PMID: 16402116]

[21] Karolewicz, B.; Klimek, V.; Zhu, H.; Szebeni, K.; Nail, E.; Stockmeier, C.A.; Johnson, L.; Ordway, G.A. Effects of depression, cigarette smoking, and age on monoamine oxidase B in amygdaloid nuclei. *Brain Res.,* **2005**, *1043*(1-2), 57-64. [http://dx.doi.org/10.1016/j.brainres.2005.02.043] [PMID: 15862518]

[22] Fowler, J.S.; Volkow, N.D.; Wang, G.J.; Logan, J.; Pappas, N.; Shea, C.; MacGregor, R. Age-related increases in brain monoamine oxidase B in living healthy human subjects. *Neurobiol. Aging,* **1997**, *18*(4), 431-435. [http://dx.doi.org/10.1016/S0197-4580(97)00037-7] [PMID: 9330975]

[23] Nicotra, A.; Pierucci, F.; Parvez, H.; Senatori, O. Monoamine oxidase expression during development and aging. *Neurotoxicology,* **2004**, *25*(1-2), 155-165. [http://dx.doi.org/10.1016/S0161-813X(03)00095-0] [PMID: 14697890]

[24] Morelli, M.; Di Paolo, T.; Wardas, J.; Calon, F.; Xiao, D.; Schwarzschild, M.A. Role of adenosine A2A receptors in parkinsonian motor impairment and l-DOPA-induced motor complications. *Prog. Neurobiol.,* **2007**, *83*(5), 293-309. [http://dx.doi.org/10.1016/j.pneurobio.2007.07.001] [PMID: 17826884]

[25] Pinna, A.; Wardas, J.; Simola, N.; Morelli, M. New therapies for the treatment of Parkinson's disease: adenosine A2A receptor antagonists. *Life Sci.,* **2005**, *77*(26), 3259-3267. [http://dx.doi.org/10.1016/j.lfs.2005.04.029] [PMID: 15979104]

[26] Xu, K.; Bastia, E.; Schwarzschild, M. Therapeutic potential of adenosine A(2A) receptor antagonists in Parkinson's disease. *Pharmacol. Ther.,* **2005**, *105*(3), 267-310. [http://dx.doi.org/10.1016/j.pharmthera.2004.10.007] [PMID: 15737407]

[27] Ferré, S.; Fredholm, B.B.; Morelli, M.; Popoli, P.; Fuxe, K. Adenosine-dopamine receptor-receptor interactions as an integrative mechanism in the basal ganglia. *Trends Neurosci.,* **1997**, *20*(10), 482-487. [http://dx.doi.org/10.1016/S0166-2236(97)01096-5] [PMID: 9347617]

[28] Kanda, T.; Jackson, M.J.; Smith, L.A.; Pearce, R.K.; Nakamura, J.; Kase, H.; Kuwana, Y.; Jenner, P. Adenosine A2A antagonist: a novel antiparkinsonian agent that does not provoke dyskinesia in parkinsonian monkeys. *Ann. Neurol.,* **1998**, *43*(4), 507-513. [http://dx.doi.org/10.1002/ana.410430415] [PMID: 9546333]

[29] Chen, J.F.; Moratalla, R.; Impagnatiello, F.; Grandy, D.K.; Cuellar, B.; Rubinstein, M.; Beilstein, M.A.; Hackett, E.; Fink, J.S.; Low, M.J.; Ongini, E.; Schwarzschild, M.A. The role of the D(2) dopamine receptor (D(2)R) in A(2A) adenosine receptor (A(2A)R)-mediated behavioral and cellular responses as revealed by A(2A) and D(2) receptor knockout mice. *Proc. Natl. Acad. Sci. USA,* **2001**, *98*(4), 1970-1975. [http://dx.doi.org/10.1073/pnas.98.4.1970] [PMID: 11172060]

[30] Petzer, J.P.; Steyn, S.; Castagnoli, K.P.; Chen, J.F.; Schwarzschild, M.A.; Van der Schyf, C.J.; Castagnoli, N. Inhibition of monoamine oxidase B by selective adenosine A2A receptor antagonists. *Bioorg. Med. Chem.,* **2003**, *11*(7), 1299-1310. [http://dx.doi.org/10.1016/S0968-0896(02)00648-X] [PMID: 12628657]

[31] Pretorius, J.; Malan, S.F.; Castagnoli, N., Jr; Bergh, J.J.; Petzer, J.P. Dual inhibition of monoamine oxidase B and antagonism of the adenosine A(2A) receptor by (E,E)-8-(4-phenylbutadien-1-yl) caffeine analogues. *Bioorg. Med. Chem.,* **2008**, *16*(18), 8676-8684. [http://dx.doi.org/10.1016/j.bmc.2008.07.088] [PMID: 18723354]

[32] Ascherio, A.; Zhang, S.M.; Hernán, M.A.; Kawachi, I.; Colditz, G.A.; Speizer, F.E.; Willett, W.C. Prospective study of caffeine consumption and risk of Parkinson's disease in men and women.

Ann. Neurol., **2001**, *50*(1), 56-63. [http://dx.doi.org/10.1002/ana.1052] [PMID: 11456310]

[33] Ross, G.W.; Abbott, R.D.; Petrovitch, H.; Morens, D.M.; Grandinetti, A.; Tung, K.H.; Tanner, C.M.; Masaki, K.H.; Blanchette, P.L.; Curb, J.D.; Popper, J.S.; White, L.R. Association of coffee and caffeine intake with the risk of Parkinson disease. *JAMA,* **2000**, *283*(20), 2674-2679. [http://dx.doi.org/10.1001/jama.283.20.2674] [PMID: 10819950]

[34] Powers, K.M.; Kay, D.M.; Factor, S.A.; Zabetian, C.P.; Higgins, D.S.; Samii, A.; Nutt, J.G.; Griffith, A.; Leis, B.; Roberts, J.W.; Martinez, E.D.; Montimurro, J.S.; Checkoway, H.; Payami, H. Combined effects of smoking, coffee, and NSAIDs on Parkinson's disease risk. *Mov. Disord.,* **2008**, *23*(1), 88-95. [http://dx.doi.org/10.1002/mds.21782] [PMID: 17987647]

[35] Chen, J.F.; Steyn, S.; Staal, R.; Petzer, J.P.; Xu, K.; Van Der Schyf, C.J.; Castagnoli, K.; Sonsalla, P.K.; Castagnoli, N., Jr; Schwarzschild, M.A. 8-(3-Chlorostyryl)caffeine may attenuate MPTP neurotoxicity through dual actions of monoamine oxidase inhibition and A2A receptor antagonism. *J. Biol. Chem.,* **2002**, *277*(39), 36040-36044. [http://dx.doi.org/10.1074/jbc.M206830200] [PMID: 12130655]

[36] Jacobson, K.A.; Gallo-Rodriguez, C.; Melman, N.; Fischer, B.; Maillard, M.; van Bergen, A.; van Galen, P.J.; Karton, Y. Structure-activity relationships of 8-styrylxanthines as A2-selective adenosine antagonists. *J. Med. Chem.,* **1993**, *36*(10), 1333-1342. [http://dx.doi.org/10.1021/jm00062a005] [PMID: 8496902]

[37] Müller, C.E.; Geis, U.; Hipp, J.; Schobert, U.; Frobenius, W.; Pawłowski, M.; Suzuki, F.; Sandoval-Ramírez, J. Synthesis and structure-activity relationships of 3,7-dimethyl-1-propargylxanthine derivatives, A2A-selective adenosine receptor antagonists. *J. Med. Chem.,* **1997**, *40*(26), 4396-4405. [http://dx.doi.org/10.1021/jm970515+] [PMID: 9435909]

[38] Rivara, S.; Piersanti, G.; Bartoccini, F.; Diamantini, G.; Pala, D.; Riccioni, T.; Stasi, M.A.; Cabri, W.; Borsini, F.; Mor, M.; Tarzia, G.; Minetti, P. Synthesis of (E)-8-(3-chlorostyryl)caffeine analogues leading to 9-deazaxanthine derivatives as dual A(2A) antagonists/MAO-B inhibitors. *J. Med. Chem.,* **2013**, *56*(3), 1247-1261. [http://dx.doi.org/10.1021/jm301686s] [PMID: 23281824]

[39] Stössel, A.; Schlenk, M.; Hinz, S.; Küppers, P.; Heer, J.; Gütschow, M.; Müller, C.E. Dual targeting of adenosine A(2A) receptors and monoamine oxidase B by 4H-3,1-benzothiazin-4-ones. *J. Med. Chem.,* **2013**, *56*(11), 4580-4596. [http://dx.doi.org/10.1021/jm400336x] [PMID: 23631427]

[40] Gütschow, M.; Schlenk, M.; Gäb, J.; Paskaleva, M.; Alnouri, M.W.; Scolari, S.; Iqbal, J.; Müller, C.E. Benzothiazinones: a novel class of adenosine receptor antagonists structurally unrelated to xanthine and adenine derivatives. *J. Med. Chem.,* **2012**, *55*(7), 3331-3341. [http://dx.doi.org/10.1021/jm300029s] [PMID: 22409573]

[41] Gaspar, A.; Matos, M.J.; Garrido, J.; Uriarte, E.; Borges, F. Chromone: a valid scaffold in medicinal chemistry. *Chem. Rev.,* **2014**, *114*(9), 4960-4992. [http://dx.doi.org/10.1021/cr400265z] [PMID: 24555663]

[42] Langmead, C.J.; Andrews, S.P.; Congreve, M.; Errey, J.C.; Hurrell, E.; Marshall, F.H.; Mason, J.S.; Richardson, C.M.; Robertson, N.; Zhukov, A.; Weir, M. Identification of novel adenosine A(2A) receptor antagonists by virtual screening. *J. Med. Chem.,* **2012**, *55*(5), 1904-1909. [http://dx.doi.org/10.1021/jm201455y] [PMID: 22250781]

[43] Lounkine, E.; Wawer, M.; Wassermann, A.M.; Bajorath, J. SARANEA: a freely available program to mine structure-activity and structure-selectivity relationship information in compound data sets. *J. Chem. Inf. Model.,* **2010**, *50*(1), 68-78. [http://dx.doi.org/10.1021/ci900416a] [PMID: 20053000]

[44] Durant, J.L.; Leland, B.A.; Henry, D.R.; Nourse, J.G. Reoptimization of MDL keys for use in drug discovery. *J. Chem. Inf. Comput. Sci.,* **2002**, *42*(6), 1273-1280. [http://dx.doi.org/10.1021/ci010132r] [PMID: 12444722]

[45] Steinbeck, C.; Han, Y.; Kuhn, S.; Horlacher, O.; Luttmann, E.; Willighagen, E. The chemistry development kit (CDK): an open-source Java library for Chemo- and Bioinformatics. *J. Chem. Inf. Comput. Sci.,* **2003**, *43*(2), 493-500. [http://dx.doi.org/10.1021/ci025584y] [PMID: 12653513]

[46] Steinbeck, C.; Hoppe, C.; Kuhn, S.; Floris, M.; Guha, R.; Willighagen, E.L. Recent developments of the chemistry development kit (CDK) - an open-source java library for chemo- and bioinformatics. *Curr. Pharm. Des.,* **2006**, *12*(17), 2111-2120. [http://dx.doi.org/10.2174/138161206777585274] [PMID: 16796559]

[47] Wawer, M.; Lounkine, E.; Wassermann, A.M.; Bajorath, J. Data structures and computational tools for the extraction of SAR information from large compound sets. *Drug Discov. Today,* **2010**, *15*(15-16), 630-639. [http://dx.doi.org/10.1016/j.drudis.2010.06.004] [PMID: 20547243]

[48] Stumpfe, D.; Bajorath, J. Methods for SAR visualization. *RSC Adv.,* **2012**, *2*, 369-378. [http://dx.doi.org/10.1039/C1RA00924A]

[49] Wawer, M.; Peltason, L.; Weskamp, N.; Teckentrup, A.; Bajorath, J. Structure-activity relationship anatomy by network-like similarity graphs and local structure-activity relationship indices. *J. Med. Chem.,* **2008**, *51*(19), 6075-6084. [http://dx.doi.org/10.1021/jm800867g] [PMID: 18798611]

[50] Peltason, L.; Bajorath, J. SAR index: quantifying the nature of structure-activity relationships. *J. Med. Chem.,* **2007**, *50*(23), 5571-5578. [http://dx.doi.org/10.1021/jm0705713] [PMID: 17902636]

[51] Harrington, E.C. The desirability function. *Ind. Quality Control,* **1965**, *21*(10), 494-498.

[52] Derringer, G.; Suich, R. Simultaneous optimization of several response variables. *J. Qual. Technol.,* **1980**, *12*(4), 214-219.

[53] Mayo, S.L.; Olafson, B.D.; Goddard, W.A. DREIDING: a generic force field for molecular simulations. *J. Phys. Chem.,* **1990**, *94*(26), 8897-8909. [http://dx.doi.org/10.1021/j100389a010]

[54] Pettersen, E.F.; Goddard, T.D.; Huang, C.C.; Couch, G.S.; Greenblatt, D.M.; Meng, E.C.; Ferrin, T.E. UCSF Chimera--a visualization system for exploratory research and analysis. *J. Comput. Chem.,* **2004**, *25*(13), 1605-1612. [http://dx.doi.org/10.1002/jcc.20084] [PMID: 15264254]

[55] Lang, P.T.; Brozell, S.R.; Mukherjee, S.; Pettersen, E.F.; Meng, E.C.; Thomas, V.; Rizzo, R.C.; Case, D.A.; James, T.L.; Kuntz, I.D. DOCK 6: combining techniques to model RNA-small molecule complexes. *RNA,* **2009**, *15*(6), 1219-1230. [http://dx.doi.org/10.1261/rna.1563609] [PMID: 19369428]

[56] Mukherjee, S.; Balius, T.E.; Rizzo, R.C. Docking validation resources: protein family and ligand flexibility experiments. *J. Chem. Inf. Model.,* **2010**, *50*(11), 1986-2000. [http://dx.doi.org/10.1021/ci1001982] [PMID: 21033739]

[57] Gaspar, A.; Reis, J.; Kachler, S.; Paoletta, S.; Uriarte, E.; Klotz, K.N.; Moro, S.; Borges, F. Discovery of novel A3 adenosine receptor ligands based on chromone scaffold. *Biochem. Pharmacol.,* **2012**, *84*(1), 21-29. [http://dx.doi.org/10.1016/j.bcp.2012.03.007] [PMID: 22433284]

[58] Gaspar, A.; Reis, J.; Fonseca, A.; Milhazes, N.; Viña, D.; Uriarte, E.; Borges, F. Chromone 3-phenylcarboxamides as potent and selective MAO-B inhibitors. *Bioorg. Med. Chem. Lett.,* **2011**, *21*(2), 707-709. [http://dx.doi.org/10.1016/j.bmcl.2010.11.128] [PMID: 21194943]

[59] Alcaro, S.; Gaspar, A.; Ortuso, F.; Milhazes, N.; Orallo, F.; Uriarte, E.; Yáñez, M.; Borges, F. Chromone-2- and -3-carboxylic acids inhibit differently monoamine oxidases A and B. *Bioorg. Med. Chem. Lett.,* **2010**, *20*(9), 2709-2712. [http://dx.doi.org/10.1016/j.bmcl.2010.03.081] [PMID: 20382016]

[60] Gaspar, A.; Silva, T.; Yáñez, M.; Vina, D.; Orallo, F.; Ortuso, F.; Uriarte, E.; Alcaro, S.; Borges, F. Chromone, a privileged scaffold for the development of monoamine oxidase inhibitors. *J. Med. Chem.,* **2011**, *54*(14), 5165-5173. [http://dx.doi.org/10.1021/jm2004267] [PMID: 21696156]

[61] Lenzi, O.; Colotta, V.; Catarzi, D.; Varano, F.; Filacchioni, G.; Martini, C.; Trincavelli, L.; Ciampi, O.; Varani, K.; Marighetti, F.; Morizzo, E.; Moro, S. 4-amido-2-aryl-1,2,4-triazolo[4,3-a]quinoxalin-1-ones as new potent and selective human A3 adenosine receptor antagonists. synthesis, pharmacological evaluation, and ligand-receptor modeling studies. *J. Med. Chem.,* **2006**, *49*(13), 3916-3925. [http://dx.doi.org/10.1021/jm060373w] [PMID: 16789747]

[62] Da Settimo, F.; Primofiore, G.; Taliani, S.; Marini, A.M.; La Motta, C.; Simorini, F.; Salerno, S.; Sergianni, V.; Tuccinardi, T.; Martinelli, A.; Cosimelli, B.; Greco, G.; Novellino, E.; Ciampi, O.; Trincavelli, M.L.; Martini, C. 5-amino-2-phenyl[1,2,3]triazolo[1,2-a][1,2,4]benzotriazin-1-one: a versatile scaffold to obtain potent and selective A3 adenosine receptor antagonists. *J. Med. Chem.,* **2007**, *50*(23), 5676-5684. [http://dx.doi.org/10.1021/jm0708376] [PMID: 17927167]

[63] Colotta, V.; Catarzi, D.; Varano, F.; Capelli, F.; Lenzi, O.; Filacchioni, G.; Martini, C.; Trincavelli, L.; Ciampi, O.; Pugliese, A.M.; Pedata, F.; Schiesaro, A.; Morizzo, E.; Moro, S. New 2-arylpyrazolo[3,4-c]quinoline derivatives as potent and selective human A3 adenosine receptor antagonists. Synthesis, pharmacological evaluation, and ligand-receptor modeling studies. *J. Med. Chem.,* **2007**, *50*(17), 4061-4074. [http://dx.doi.org/10.1021/jm070123v] [PMID: 17665891]

[64] Cheong, S.L.; Dolzhenko, A.; Kachler, S.; Paoletta, S.; Federico, S.; Cacciari, B.; Dolzhenko, A.; Klotz, K.N.; Moro, S.; Spalluto, G.; Pastorin, G. The significance of 2-furyl ring substitution with a 2-(para-substituted) aryl group in a new series of pyrazolo-triazolo-pyrimidines as potent and highly selective hA(3) adenosine receptors antagonists: new insights into structure-affinity relationship and receptor-antagonist recognition. *J. Med. Chem.,* **2010**, *53*(8), 3361-3375. [http://dx.doi.org/10.1021/jm100049f] [PMID: 20307065]

[65] Michielan, L.; Bolcato, C.; Federico, S.; Cacciari, B.; Bacilieri, M.; Klotz, K.N.; Kachler, S.; Pastorin, G.; Cardin, R.; Sperduti, A.; Spalluto, G.; Moro, S. Combining selectivity and affinity predictions using an integrated Support Vector Machine (SVM) approach: An alternative tool to discriminate between the human adenosine A(2A) and A(3) receptor pyrazolo-triazolo-pyrimidine antagonists binding sites. *Bioorg. Med. Chem.,* **2009**, *17*(14), 5259-5274. [http://dx.doi.org/10.1016/j.bmc.2009.05.038] [PMID: 19501513]

[66] Cosimelli, B.; Greco, G.; Ehlardo, M.; Novellino, E.; Da Settimo, F.; Taliani, S.; La Motta, C.; Bellandi, M.; Tuccinardi, T.; Martinelli, A.; Ciampi, O.; Trincavelli, M.L.; Martini, C. Derivatives of 4-amino-6-hydroxy-2-mercaptopyrimidine as novel, potent, and selective A3 adenosine receptor antagonists. *J. Med. Chem.,* **2008**, *51*(6), 1764-1770. [http://dx.doi.org/10.1021/jm701159t] [PMID: 18269230]

[67] Novellino, E.; Cosimelli, B.; Ehlardo, M.; Greco, G.; Iadanza, M.; Lavecchia, A.; Rimoli, M.G.; Sala, A.; Da Settimo, A.; Primofiore, G.; Da Settimo, F.; Taliani, S.; La Motta, C.; Klotz, K.N.; Tuscano, D.; Trincavelli, M.L.; Martini, C. 2-(Benzimidazol-2-yl)quinoxalines: a novel class of selective antagonists at human A(1) and A(3) adenosine receptors designed by 3D database searching. *J. Med. Chem.,* **2005**, *48*(26), 8253-8260. [http://dx.doi.org/10.1021/jm050792d] [PMID: 16366607]

[68] Colotta, V.; Catarzi, D.; Varano, F.; Lenzi, O.; Filacchioni, G.; Martini, C.; Trincavelli, L.; Ciampi, O.; Traini, C.; Pugliese, A.M.; Pedata, F.; Morizzo, E.; Moro, S. Synthesis, ligand-receptor modeling studies and pharmacological evaluation of novel 4-modified-2-aryl-1,2,4-triazolo[4,3-a]quinoxalin-1-one derivatives as potent and selective human A3 adenosine receptor antagonists. *Bioorg. Med. Chem.,* **2008**, *16*(11), 6086-6102. [http://dx.doi.org/10.1016/j.bmc.2008.04.039] [PMID: 18468446]

[69] Lambertucci, C.; Antonini, I.; Buccioni, M.; Dal Ben, D.; Kachare, D.D.; Volpini, R.; Klotz, K.N.; Cristalli, G. 8-Bromo-9-alkyl adenine derivatives as tools for developing new adenosine A2A and A2B receptors ligands. *Bioorg. Med. Chem.,* **2009**, *17*(7), 2812-2822. [http://dx.doi.org/10.1016/j.bmc.2009.02.030] [PMID: 19282184]

[70] Colotta, V.; Lenzi, O.; Catarzi, D.; Varano, F.; Filacchioni, G.; Martini, C.; Trincavelli, L.; Ciampi, O.; Pugliese, A.M.; Traini, C.; Pedata, F.; Morizzo, E.; Moro, S. Pyrido[2,3-e]-1,2,4-triazolo [4,3-a]pyrazin-1-one as a new scaffold to develop potent and selective human A3 adenosine receptor antagonists. Synthesis, pharmacological evaluation, and ligand-receptor modeling studies. *J. Med. Chem.,* **2009**, *52*(8), 2407-2419. [http://dx.doi.org/10.1021/jm8014876] [PMID: 19301821]

[71] Taliani, S.; La Motta, C.; Mugnaini, L.; Simorini, F.; Salerno, S.; Marini, A.M.; Da Settimo, F.; Cosconati, S.; Cosimelli, B.; Greco, G.; Limongelli, V.; Marinelli, L.; Novellino, E.; Ciampi, O.; Daniele, S.; Trincavelli, M.L.; Martini, C. Novel N2-substituted pyrazolo[3,4-d]pyrimidine adenosine A3 receptor antagonists: inhibition of A3-mediated human glioblastoma cell proliferation. *J. Med. Chem.,* **2010**, *53*(10), 3954-3963. [http://dx.doi.org/10.1021/jm901785w] [PMID: 20408530]

[72] Michielan, L.; Bacilieri, M.; Schiesaro, A.; Bolcato, C.; Pastorin, G.; Spalluto, G.; Cacciari, B.; Klotz, K.N.; Kaseda, C.; Moro, S. Linear and nonlinear 3D-QSAR approaches in tandem with ligand-based homology modeling as a computational strategy to depict the pyrazolo-triazolo-pyrimidine antagonists binding site of the human adenosine A2A receptor. *J. Chem. Inf. Model.,* **2008**, *48*(2), 350-363. [http://dx.doi.org/10.1021/ci700300w] [PMID: 18215030]

[73] Michielan, L.; Stephanie, F.; Terfloth, L.; Hristozov, D.; Cacciari, B.; Klotz, K.N.; Spalluto, G.; Gasteiger, J.; Moro, S. Exploring potency and selectivity receptor antagonist profiles using a multilabel classification approach: the human adenosine receptors as a key study. *J. Chem. Inf. Model.,* **2009**, *49*(12), 2820-2836. [http://dx.doi.org/10.1021/ci900311j] [PMID: 19908874]

[74] Moro, S.; Bacilieri, M.; Cacciari, B.; Bolcato, C.; Cusan, C.; Pastorin, G.; Klotz, K.N.; Spalluto, G. The application of a 3D-QSAR (autoMEP/PLS) approach as an efficient pharmacodynamic-driven filtering method for small-sized virtual library: application to a lead optimization of a human A3 adenosine receptor antagonist. *Bioorg. Med. Chem.,* **2006**, *14*(14), 4923-4932. [http://dx.doi.org/10.1016/j.bmc.2006.03.010] [PMID: 16564691]

[75] Klotz, K.N.; Kachler, S.; Lambertucci, C.; Vittori, S.; Volpini, R.; Cristalli, G. 9-Ethyladenine derivatives as adenosine receptor antagonists: 2- and 8-substitution results in distinct selectivities. *Naunyn Schmiedebergs Arch. Pharmacol.,* **2003**, *367*(6), 629-634. [http://dx.doi.org/10.1007/s00210-003-0749-9] [PMID: 12734636]

[76] Cristalli, G.; Camaioni, E.; Costanzi, S.; Vittori, S.; Volpini, R.; Klotz, K.N. Characterization of potent ligands at human recombinant adenosine receptors. *Drug Dev. Res.,* **1998**, *45*(3-4), 176-181. [http://dx.doi.org/10.1002/(SICI)1098-2299(199811/12)45:3/4<176::AID-DDR14>3.0.CO;2-G]

[77] Taliani, S.; Trincavelli, M.L.; Cosimelli, B.; Laneri, S.; Severi, E.; Barresi, E.; Pugliesi, I.; Daniele, S.; Giacomelli, C.; Greco, G.; Novellino, E.; Martini, C.; Da Settimo, F. Modulation of A2B adenosine receptor by 1-Benzyl-3-ketoindole derivatives. *Eur. J. Med. Chem.,* **2013**, *69*, 331-337. [http://dx.doi.org/10.1016/j.ejmech.2013.09.001] [PMID: 24077183]

[78] Helguera, A.M.; Pérez-Garrido, A.; Gaspar, A.; Reis, J.; Cagide, F.; Vina, D.; Cordeiro, M.N.; Borges, F. Combining QSAR classification models for predictive modeling of human monoamine oxidase inhibitors. *Eur. J. Med. Chem.,* **2013**, *59*, 75-90. [http://dx.doi.org/10.1016/j.ejmech.2012.10.035] [PMID: 23207409]

[79] Chimenti, F.; Fioravanti, R.; Bolasco, A.; Chimenti, P.; Secci, D.; Rossi, F.; Yáñez, M.; Orallo, F.; Ortuso, F.; Alcaro, S. Chalcones: a valid scaffold for monoamine oxidases inhibitors. *J. Med. Chem.,* **2009**, *52*(9), 2818-2824. [http://dx.doi.org/10.1021/jm801590u] [PMID: 19378991]

[80] Chimenti, F.; Secci, D.; Bolasco, A.; Chimenti, P.; Bizzarri, B.; Granese, A.; Carradori, S.; Yáñez, M.; Orallo, F.; Ortuso, F.; Alcaro, S. Synthesis, molecular modeling, and selective inhibitory activity against human monoamine oxidases of 3-carboxamido-7-substituted coumarins. *J. Med. Chem.,* **2009**, *52*(7), 1935-1942. [http://dx.doi.org/10.1021/jm801496u] [PMID: 19267475]

[81] Chimenti, F.; Carradori, S.; Secci, D.; Bolasco, A.; Chimenti, P.; Granese, A.; Bizzarri, B. Synthesis and biological evaluation of novel conjugated coumarin-thiazole systems. *J. Heterocycl. Chem.,* **2009**, *46*, 575-578. [http://dx.doi.org/10.1002/jhet.110]

[82] Santana, L.; González-Díaz, H.; Quezada, E.; Uriarte, E.; Yáñez, M.; Viña, D.; Orallo, F. Quantitative structure-activity relationship and complex network approach to monoamine oxidase A and B inhibitors. *J. Med. Chem.,* **2008**, *51*(21), 6740-6751. [http://dx.doi.org/10.1021/jm800656v] [PMID: 18834112]

[83] Matos, M.J.; Viña, D.; Quezada, E.; Picciau, C.; Delogu, G.; Orallo, F.; Santana, L.; Uriarte, E. A new series of 3-phenylcoumarins as potent and selective MAO-B inhibitors. *Bioorg. Med. Chem. Lett.,* **2009**, *19*(12), 3268-3270. [http://dx.doi.org/10.1016/j.bmcl.2009.04.085] [PMID: 19423346]

[84] Chimenti, F.; Secci, D.; Bolasco, A.; Chimenti, P.; Granese, A.; Carradori, S.; Maccioni, E.; Cardia, M.C.; Yáñez, M.; Orallo, F.; Alcaro, S.; Ortuso, F.; Cirilli, R.; Ferretti, R.; Distinto, S.; Kirchmair, J.; Langer, T. Synthesis, semipreparative HPLC separation, biological evaluation, and 3D-QSAR of hydrazothiazole derivatives as human monoamine oxidase B inhibitors. *Bioorg. Med. Chem.,* **2010**, *18*(14), 5063-5070. [http://dx.doi.org/10.1016/j.bmc.2010.05.070] [PMID: 20579890]

[85] Chimenti, F.; Secci, D.; Bolasco, A.; Chimenti, P.; Granese, A.; Carradori, S.; Yáñez, M.; Orallo, F.; Sanna, M.L.; Gallinella, B.; Cirilli, R. Synthesis, stereochemical separation, and biological evaluation of selective inhibitors of human MAO-B: 1-(4-arylthiazol-2-yl)-2-(3-methylcyclohexylidene)hydrazines. *J. Med.*

Chem., **2010**, *53*(17), 6516-6520. [http://dx.doi.org/10.1021/jm100120s] [PMID: 20715818]

[86] Chimenti, F.; Secci, D.; Bolasco, A.; Chimenti, P.; Granese, A.; Carradori, S.; D'Ascenzio, M.; Yáñez, M.; Orallo, F. Synthesis and selective inhibition of human monoamine oxidases of a large scaffold of (4,5-substituted-thiazol-2-yl)hydrazones. *MedChem. Comm.,* **2010**, *1*, 61-72. [http://dx.doi.org/10.1039/c0md00014k]

[87] Desideri, N.; Bolasco, A.; Fioravanti, R.; Monaco, L.P.; Orallo, F.; Yáñez, M.; Ortuso, F.; Alcaro, S. Homoisoflavonoids: natural scaffolds with potent and selective monoamine oxidase-B inhibition properties. *J. Med. Chem.,* **2011**, *54*(7), 2155-2164. [http://dx.doi.org/10.1021/jm1013709] [PMID: 21405131]

[88] Fioravanti, R.; Bolasco, A.; Manna, F.; Rossi, F.; Orallo, F.; Yáñez, M.; Vitali, A.; Ortuso, F.; Alcaro, S. Synthesis and molecular modelling studies of prenylated pyrazolines as MAO-B inhibitors. *Bioorg. Med. Chem. Lett.,* **2010**, *20*(22), 6479-6482. [http://dx.doi.org/10.1016/j.bmcl.2010.09.061] [PMID: 20934874]

[89] Maccioni, E.; Alcaro, S.; Orallo, F.; Cardia, M.C.; Distinto, S.; Costa, G.; Yáñez, M.; Sanna, M.L.; Vigo, S.; Meleddu, R.; Secci, D. Synthesis of new 3-aryl-4,5-dihydropyrazole-1-carbothioamide derivatives. An investigation on their ability to inhibit monoamine oxidase. *Eur. J. Med. Chem.,* **2010**, *45*(10), 4490-4498. [http://dx.doi.org/10.1016/j.ejmech.2010.07.009] [PMID: 20702005]

[90] Matos, M.J.; Viña, D.; Janeiro, P.; Borges, F.; Santana, L.; Uriarte, E. New halogenated 3-phenylcoumarins as potent and selective MAO-B inhibitors. *Bioorg. Med. Chem. Lett.,* **2010**, *20*(17), 5157-5160. [http://dx.doi.org/10.1016/j.bmcl.2010.07.013] [PMID: 20659799]

[91] Delogu, G.; Picciau, C.; Ferino, G.; Quezada, E.; Podda, G.; Uriarte, E.; Viña, D. Synthesis, human monoamine oxidase inhibitory activity and molecular docking studies of 3-heteroarylcoumarin derivatives. *Eur. J. Med. Chem.,* **2011**, *46*(4), 1147-1152. [http://dx.doi.org/10.1016/j.ejmech.2011.01.033] [PMID: 21316817]

[92] Matos, M.J.; Terán, C.; Pérez-Castillo, Y.; Uriarte, E.; Santana, L.; Viña, D. Synthesis and study of a series of 3-arylcoumarins as potent and selective monoamine oxidase B inhibitors. *J. Med. Chem.,* **2011**, *54*(20), 7127-7137. [http://dx.doi.org/10.1021/jm200716y] [PMID: 21923181]

[93] Yáñez, M.; Fraiz, N.; Cano, E.; Orallo, F. Inhibitory effects of cis- and trans-resveratrol on noradrenaline and 5-hydroxytryptamine uptake and on monoamine oxidase activity. *Biochem. Biophys. Res. Commun.,* **2006**, *344*(2), 688-695. [http://dx.doi.org/10.1016/j.bbrc.2006.03.190] [PMID: 16631124]

[94] Tropsha, A. Best practices for QSAR model development, validation, and exploitation. *Mol. Inform.,* **2010**, *29*(6-7), 476-488. [http://dx.doi.org/10.1002/minf.201000061] [PMID: 27463326]

[95] ChemAxon. *J. Chem for Excel.,* **2012**.

[96] ChemAxon. Standardizer, **2012**.

[97] Solov'ev, V.P.; Varnek, A. **2010**, pp. (Editor of the Structure Data Files)

[98] Varnek, A.; Fourches, D.; Hoonakker, F.; Solov'ev, V.P. Substructural fragments: an universal language to encode reactions, molecular and supramolecular structures. *J. Comput. Aided Mol. Des.,* **2005**, *19*(9-10), 693-703. [http://dx.doi.org/10.1007/s10822-005-9008-0] [PMID: 16292611]

[99] Varnek, A.; Fourches, D.; Horvath, D.; Klimchuk, O.; Gaudin, C.; Vayer, P.; Solov'ev, V.; Hoonakker, F.; Tetko, I. G., M. ISIDA - platform for virtual screening based on fragment and pharmacophoric descriptors. *Curr. Comput. Aided Drug Des.,* **2008**, *4*, 191-198. [http://dx.doi.org/10.2174/157340908785747465]

[100] Willett, P. Similarity-based virtual screening using 2D fingerprints. *Drug Discov. Today,* **2006**, *11*(23-24), 1046-1053. [http://dx.doi.org/10.1016/j.drudis.2006.10.005] [PMID: 17129822]

[101] Nasr, R.J.; Swamidass, S.J.; Baldi, P.F. Large scale study of multiple-molecule queries. *J. Cheminform.,* **2009**, *1*(1), 7. [http://dx.doi.org/10.1186/1758-2946-1-7] [PMID: 20298525]

[102] Truchon, J.F.; Bayly, C.I. Evaluating virtual screening methods: good and bad metrics for the "early recognition" problem. *J. Chem. Inf. Model.,* **2007**, *47*(2), 488-508. [http://dx.doi.org/10.1021/ci600426e] [PMID: 17288412]

[103] Kirchmair, J.; Markt, P.; Distinto, S.; Wolber, G.; Langer, T. Evaluation of the performance of 3D virtual screening protocols: RMSD comparisons, enrichment assessments, and decoy selection--what can we learn from earlier mistakes? *J. Comput. Aided Mol. Des.,* **2008**, *22*(3-4), 213-228. [http://dx.doi.org/10.1007/s10822-007-9163-6] [PMID: 18196462]

[104] Wawer, M.; Bajorath, J. Systematic extraction of structure-activity relationship information from biological screening data. *ChemMedChem,* **2009**, *4*(9), 1431-1438. [http://dx.doi.org/10.1002/cmdc.200900222] [PMID: 19621333]

[105] Doré, A.S.; Robertson, N.; Errey, J.C.; Ng, I.; Hollenstein, K.; Tehan, B.; Hurrell, E.; Bennett, K.; Congreve, M.; Magnani, F.; Tate, C.G.; Weir, M.; Marshall, F.H. Structure of the adenosine A(2A) receptor in complex with ZM241385 and the xanthines XAC and caffeine. *Structure,* **2011**, *19*(9), 1283-1293. [http://dx.doi.org/10.1016/j.str.2011.06.014] [PMID: 21885291]

[106] Binda, C.; Wang, J.; Pisani, L.; Caccia, C.; Carotti, A.; Salvati, P.; Edmondson, D.E.; Mattevi, A. Structures of human monoamine oxidase B complexes with selective noncovalent inhibitors: safinamide and coumarin analogs. *J. Med. Chem.,* **2007**, *50*(23), 5848-5852. [http://dx.doi.org/10.1021/jm070677y] [PMID: 17915852]

[107] Huang, N.; Shoichet, B.K.; Irwin, J.J. Benchmarking sets for molecular docking. *J. Med. Chem.,* **2006**, *49*(23), 6789-6801. [http://dx.doi.org/10.1021/jm0608356] [PMID: 17154509]